There may be differences between this version and the published version. You are advised to consult the publisher's version if you wish to cite from it.

http://eprints.gla.ac.uk/173403/

Deposited on: 21 January 2019

Dalton Transactions

Accepted Manuscript

Strategic Synthesis of [Cu₂], [Cu₄] and [Cu₅] Complexes: Inhibition and Triggering of Ligand Arm Hydrolysis and Self-aggregation by Chosen Ancillary Bridges

Manisha Das,[a] Angelos B. Canaj,[b] Valerio Bertolasi,[c] Mark Murrie,[b] Debashis Ray[*a]

[a]*Department of Chemistry, Indian Institute of Technology, Kharagpur 721302, India*

[b]*WestCHEM, School of Chemistry, University of Glasgow, University Avenue, Glasgow, G12 8QQ, UK.*

[c]*Dipartimento di ScienzeChimiche e Farmaceutiche, University of Ferrara, 44121 Ferrara, Italy*

Abstract

The Schiff base ligand HL1 ({2,6-bis(allylimino)methyl}-4-methylphenol) having no coordinating donor arm has been examined for its reaction medium and ancillary bridge dependent reactivity for hierarchical family of Cu^{II} complexes. The ligand showed unique reactivity pattern toward Cu^{II} in solution. The bridging nature of *in situ* generated HO^- ions in absence and presence of externally added carboxylates ($RCOO^-$; R= CF_3, C_6H_5 and CH_3) has been utilized to produce complexes $\{[Cu_2(\mu–L2)_2(H_2O)]_2[Cu_2(\mu–L2)_2(H_2O)_2](ClO_4)_6\}$ (**1**) (HL2 = 3-{(allylimino)methyl}-2-hydroxy-5-methylbenzaldehyde), $[Cu_4(\mu_4–O)(\mu–L1)_2(\mu_{1,3}–O_2CCF_3)_4]$ (**2**), $[Cu_4(\mu_4–O)(\mu–L1)_2(\mu_{1,3}–O_2CC_6H_5)_4]·H_2O$ (**3**), $[Cu_5(\mu_3–OH)_2(\mu–L1)_2(\mu_{1,3}–OAc)_2(OAc)_2(H_2O)_4][Cu_5(\mu_3–OH)_2(\mu–L1)_2(\mu_{1,3}–OAc)_2(OAc)_3(H_2O)](ClO_4)_3·2C_2H_5OH$ (**4**). Absence of carboxylate anions did not yield HO^- ions *in situ* and triggered single ligand arm hydrolysis. The formation of tetra- and pentanuclear aggregates as well as ligand hydrolyzed dinulcear products has been rationalized to identify the possible roles of carboxylate anions in solution. Detailed characterization of the complexes in the solid state and in solution have been carried out using spectroscopic measurements, X-ray crystallography, variable temperature magnetic measurements and functional behavior. In MeOH solutions at 298 K, the complexes **1-4** showed catalytic oxidation of 3,5-di-*tert*-butyl catechol (3,5-DTBCH₂) saturated with O_2 of air.

Introduction

Amine oxidases (CuAOs) containing the copper(II) ion and 2,4,5-trihydroxyphenylalanine quinone (TPQ) are now known to be responsible for the breakdown and regulation of biologically active amines in several organisms where the metal ion center does not play any redox role in catalysis.[1] The catalytic process generates aldehyde from a wide range of primary amines in the reductive half–reaction, in which Cu(II)-TPQ_{OX} reacts with amines to form the quinoneimine 'substrate Schiff base'. Next α-carbon proton abstraction leads to the quinolaldimine 'product Schiff base' responsible for release of aldehyde via hydrolysis. Quinone based Schiff bases are similar to the aldehyde-based congeners in terms of their hydrolytic susceptibility. The presence of a protein bound Cu(II) center plays the crucial role in the hydrolysis of the product Schiff base. Using synthetic transition metal ion complexes, we and others have shown that the *pH* of the medium is crucial for the coordination-induced hydrolysis and release of free amine similar to the case of CuAOs.[2] At *pH* < 7 the Schiff base substrate is prone to hydrolytic cleavage of the imine bond where protonation of the imine nitrogen atom makes the adjacent carbon electrophilic in nature for attack from a water molecule coordinated to the Cu(II) center. In this work we intend to establish the hydrolytic susceptibility of a phenol-based aldehyde Schiff base in the presence of copper(II) ions, similar to the hydrolysis of quinone Schiff base in CuAOs.

Thus, during the synthesis of multinuclear coordination compounds, it is vital to recognize and interpret the self-aggregation processes of different fragments in solution at room temperature for the creation of Cu^{II}-based compounds in a phenoxido-bridging and imine supporting environment. The role of ligand design and tuning of reaction protocol with the use of ancillary ligands in controlling the ligand stability are crucial to understand and control the aggregation process. Understanding of the processes is dependent on the knowledge of the solution stability and structure of the ligand bound mononuclear and dinuclear fragments.[3] The search for a new ligand system is in progress for the synthesis and structural identification of $[Cu_2]$ and $[Cu_4]$ complexes because of their participation in catalytic CH_4 oxidation.[4] The later species can have a μ_4-oxido core and the ligand bound Cu_4O unit is important both in industrial catalysis for substituted phenol to quinone conversion[5] and in the biological catalysis cycle of nitrous oxide reduction.[6]

In the biological realm the catechol oxidases (COs) are Cu_2-based metalloenzymes of the oxido-reductase family. They comprise a $[Cu_2]$ active site which catalyzes the two-electron oxidation of a broad range of *o*-diphenols (catechols) to the corresponding *o*-quinones,

together with the reduction of O_2 from air to water.[7] Thus a large number of copper(II)-based model fragments and complexes have been studied as models for CO in an attempt to establish the mechanism and discover efficient mimics. Different dinuclear and mononuclear copper complexes have been synthesized and examined for their efficiency towards 3,5-DTBCH$_2$ (3,5-di-*tert*-butylcatechol) oxidation.[8] The solution stability of Schiff base-bound Cu$_2$L species having several aqua coordination sites is dependent on the *pH* of the reaction medium. The presence of these species is important in synthesis for the isolation and crystallization of aggregates in the solid state. Solution *pH* and coordination of ancillary bridges replacing the aqua H_2O molecules direct the course of assembly reaction during self-aggregation of these Cu$_2$L fragments in solution. The association of two or more Cu$_2$L units can provide various multinuclear architectures, *e.g.*, cubane,[9] tetrahedron,[10] stepped cubane,[11] rhomboid,[12] double cubane[13] and cuboctahedron.[14] The outcome of reactions of a chosen Schiff base ligand system with different copper(II) salts depends on the length and plasticity of side arms with or without donor atoms, as well as on the particular reaction conditions and the solvent used. However, the exact role of each of these factors is still not well established to predict and direct the preferential aggregation process.[15] Our present effort is dedicated to examine the reactivity pattern of a new ligand system with copper(II) ions, in the environments of H_2O, ClO_4^- and RCO_2^-, for the modulation of the course of the reaction. In different solvent media and in the presence of the above-mentioned groups, the fragments CuL2 and Cu$_2$L1 (HL1 = {2,6-bis(allylimino)methyl}-4-methylphenol, HL2 = 3-{(allylimino)methyl}-2-hydroxy-5-methylbenzaldehyde) were stabilized. The presence of perchlorate anions triggers the hydrolysis of one imine arm of the ligand (Scheme 1), whereas the presence of carboxylate anions has been shown to attenuate the Schiff base hydrolysis and results in aggregation of initially formed fragments into μ_4-oxido-bridged [Cu$_4$] and double μ_3–OH bridged [Cu$_5$] complexes. We were unable to isolate any type of dinuclear complex of intact L1$^-$ from the reaction medium due to the facile 'spontaneous *in situ* self-aggregation' reactions for [Cu$_4$] and [Cu$_5$] complexes.
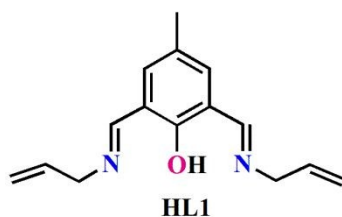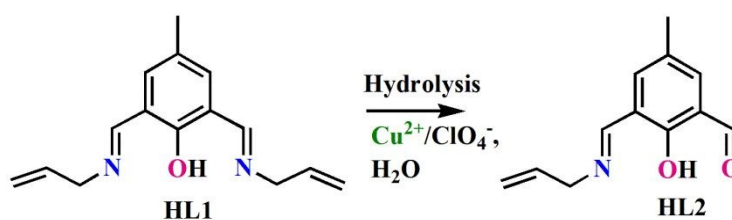

Chart 1 HL1 used in this work

We have been interested in exploring the reactivity of 2,6-bis(allylimino)methyl)-4-methylphenol (HL1; Chart 1) with Cu^{II} ions in presence of H_2O, ClO_4^- and RCO_2^-. Complexes of HL1 with transition metal ions have been unknown thus far.

Scheme 1 Partial imine arm hydrolysis

Experimental Section

Reagents and materials

The chemicals used were obtained from the following sources: Trifluroacetic acid from SRL; sodium acetate from SD Fine-chem; sodium benzoate, copper hydroxide carbonate, triethylamine from Merck, India and allyl amine from Alfa Aesar. Copper(II) perchlorate hexa-hydrate was freshly prepared by treating hydrated copper(II) carbonate (22.12 g, 0.1 mol) with 1:1 aqueous solution of perchloric acid. Sodium trifluroacetate was prepared by treating sodium hydroxide (4.00 g, 0.1 mol) and trifluroacetic acid (11.40 g, 0.1 mol) in water. 2,6-diformyl-4-methylphenol (2-hydroxy-5-methyl-benzene-1,3-dicarbaldehyde) was prepared following a modified literature procedure providing a better yield.[16] All the chemicals and solvents used in this work were of reagent grade and used as received without further purification.

Synthesis

Ligand HL1 (2,6-bis(allylimino)methyl)-4-methylphenol). 4-methyl-2,6-diformylphenol was prepared following a modified literature procedure.[16] To a MeOH solution of 4-methyl-2,6-diformylphenol (0.820 g, 5 mmol), allyl amine (1.05 g, 10 mmol) in MeOH (10 ml) was added with constant stirring and was refluxed for 2 h. Complete evaporation of the solvent in air over 12 h gave an orange oily substance, which was dried under vacuum over P_4O_{10}. The oily substance was characterized by FT-IR and NMR spectroscopy and used directly for reactions with metal ion salts without further purification. FTIR (cm^{-1}, KBr disk): 1636 (m). ^1H NMR (400 MHz, $CDCl_3$, δ ppm): 8.30–8.53 (1H, imine H), 7.26–7.65 (1H, Ar−H), 5.97−6.06 (1H, vinyl H), 5.13–5.23 (2H, vinyl H), 4.22−4.23 (2H, allyl H), 2.27 (3H, methyl

H).^{13}C NMR (100 MHz, CDCl$_3$, δ ppm): 165.04 (imine C), 124.06–163.36 (Ar C), 116.62–127.54 (alkene C), 53.93 (secondary C attached to imine N), 20.32−20.35 (methyl C).

Complexes

A common synthetic practice was followed for the preparation of **1–4** using Cu(ClO$_4$)$_2$·6H$_2$O in the absence or presence of sodium salts of three different carboxylates. Orange MeCN or MeOH solutions of HL1 on reaction with Cu(ClO$_4$)$_2$·6H$_2$O in MeOH in the absence or presence of CF$_3$COO$^-$, C$_6$H$_5$COO$^-$ and CH$_3$COO$^-$ resulted in all the four complexes.

[Cu$_2$(μ–L2)$_2$(H$_2$O)]$_2$[Cu$_2$(μ–L2)$_2$(H$_2$O)$_2$](ClO$_4$)$_6$ (1). A solution of as-prepared HL1 (*approx.* 0.24 g, 1 mmol) was dried in vacuum and the gummy mass thus obtained was re-dissolved in MeCN (10 mL). To this copper(II) perchlorate hexahydrate (0.37 g, 1 mmol) was added slowly and the resulting green solution was magnetically stirred for *ca.* 15 min, followed by reflux for 2 h. The resulting deep-green solution was filtered and kept undisturbed for slow evaporation in air. Block-shaped green crystals suitable for X-ray diffraction were obtained after three weeks. Yield: 1.22 g (54%). Micro analytical data are consistent with the molecular formula of [Cu$_2$(μ–L2)$_2$(H$_2$O)]$_2$[Cu$_2$(μ–L2)$_2$(H$_2$O)$_2$](ClO$_4$)$_6$. Anal. Calcd for C$_{72}$H$_{80}$Cu$_6$N$_6$O$_{40}$Cl$_6$ (2263.36 g mol^{-1}): C, 38.21; H, 3.56; N, 3.71. Found: C, 38.14; H, 3.53; N, 3.73. Selected FTIR bands: (KBr, cm^{-1}, vs = very strong, br = broad, s = strong, m = medium, w = weak): 3448 (br), 1629 (vs), 1554 (s), 1090 (vs), 622 (m). UV-vis spectra [λ$_{max}$, nm (ε, L mol^{-1} cm^{-1})]: (MeOH solution) 708 (76), 366 (19300), 243 (91600). Molar conductance, Λ$_M$: (MeOH solution) 230 Ω^{-1} cm^2 mol^{-1}.

[Cu$_4$(μ$_4$-O)(μ–L1)$_2$(μ$_{1,3}$–O$_2$CCF$_3$)$_4$] (2). To a stirred solution of HL1 (*approx.* 0.242 g, 1 mmol) in MeOH (10 mL) solid copper(II) perchlorate hexahydrate (0.74 g, 2 mmol) was added under stirring condition which give a light green solution. After 10 min of stirring, a MeOH solution (10 mL) of sodium trifluroacetate (0.274 g, 2 mmol) was added, resulting in a darkening of color and the stirring was continued for 2 h. The solution was then filtered, and kept in air at room temperature for slow evaporation. Green single crystals suitable for X-ray analysis were obtained after 2 days. Yield: 0.710 g (59%). Micro analytical data are consistent with the molecular formula of [Cu$_4$(μ$_4$–O)(μ–L1)$_2$(μ$_{1,3}$–O$_2$CCF$_3$)$_4$]. Anal. Calcd for C$_{38}$H$_{34}$Cu$_4$N$_4$O$_{11}$F$_{12}$ (1204.85 g mol^{-1}): C, 37.88; H, 2.84; N, 4.65. Found: C, 37.97; H, 2.80; N, 4.67. Selected FTIR bands: (KBr, cm^{-1}, vs = very strong, br = broad, s = strong, m = medium): 1688 (vs), 1636 (m), 1436 (m), 1195 (vs). UV-vis spectra [λ$_{max}$, nm (ε, L mol^{-1} cm$^-$

$^1)$]: (MeOH solution) 666 (104), 372 (8100), 261 (45400). Molar conductance, Λ_M: (MeOH solution) 34 Ω^{-1} cm^2 mol^{-1}.

[Cu$_4$(μ_4-O)(μ-L1)$_2$($\mu_{1,3}$–O$_2$CC$_6$H$_5$)$_4$]·H$_2$O (3). Complex **3** was prepared following the similar procedure as described above for **2** using sodium benzoate (0.288 g, 2 mmol) as the carboxylate source in place of sodium trifluroacetate. Block-shaped green crystals suitable for X-ray analysis were obtained after 1 week. Yield: 0.664 g (54%). Micro analytical data are consistent with the molecular formula of [Cu$_4$(μ_4-O)(μ-L1)$_2$($\mu_{1,3}$–O$_2$CC$_6$H$_5$)$_4$]·H$_2$O. Anal Calcd for C$_{58}$H$_{56}$Cu$_4$N$_4$O$_{12}$ (1255.26 g mol^{-1}): C, 55.50; H, 4.50; N, 4.46. Found: C, 55.62; H, 4.54; N, 4.44. Selected FT-IR bands: (KBr, cm^{-1}, vs = very strong, br = broad, s = strong, m = medium, w = weak): 3447 (br), 1624 (vs), 1611 (vs), 1458 (m), 1370 (vs). UV-vis spectra [λ_{max}, nm (ε, L mol^{-1} cm^{-1})]: (MeOH solution) 635 (184), 366 (16400), 259 (91100). Molar conductance, Λ_M: (MeOH solution) 27 Ω^{-1} cm^2 mol^{-1}.

[Cu$_5$(μ_3-OH)$_2$(μ-L1)$_2$($\mu_{1,3}$–OAc)$_2$(OAc)$_2$(H$_2$O)$_4$][Cu$_5$(μ_3–OH)$_2$(μ–L1)$_2$($\mu_{1,3}$–OAc)$_2$(OAc)$_3$ (H$_2$O)](ClO$_4$)$_3$·2C$_2$H$_5$OH (4). An EtOH solution (10 mL) of copper(II) perchlorate hexahydrate (0.930 g, 2.5 mmol) was added to the as-prepared 'solution of HL1' (*approx.* 0.242 g, 1 mmol) in EtOH (20 mL) with stirring and the resulting green solution was stirred for 15 min. An EtOH solution (5 mL) of sodium acetate (0.348 g, 4.25 mmol) was then added and the resulting reaction mixture was stirred for 2 h to give a dark green solution. The solution was filtered and kept for slow evaporation in air. Green block-shaped crystals suitable for X-ray structure analysis were obtained after 1 week. Yield: 1.37 g (52%). Micro analytical data are consistent with the above-mentioned formula for **4**. Anal Calcd for C$_{82}$H$_{121}$Cl$_3$Cu$_{10}$N$_8$O$_{45}$ (2680.61 g mol^{-1}): C, 36.74; H, 4.55; N, 4.18. Found: C, 36.69; H, 4.53; N, 4.17. Selected FTIR bands: (KBr, cm^{-1}, vs = very strong, br = broad, s = strong, m = medium, w = weak): 3447 (br), 1630 (m), 1564 (vs), 1412 (m), 1338 (m), 1092 (vs). UV-vis spectra [λ_{max}, nm (ε, L mol^{-1} cm^{-1})]: (MeOH solution) 670 (157), 367 (48300), 258 (238800). Molar conductance, Λ_M: (MeOH solution) 250 Ω^{-1} cm^2 mol^{-1}.

Caution! *Metal ion complexes containing organic ligands along with perchlorate counter anions are potentially explosive in nature. Therefore it is necessary to prepare only a small amount of the samples at a time for safety reasons and treat them with utmost care at all times.*

Physical Measurements

Elemental analyses (C, H and N) of the compounds were performed with a Perkin Elmer model 240C elemental analyzer. A Shimadzu UV 3100 UV–vis–NIR spectrophotometer and a PerkinElmer RX1 spectrometer were used to record the solution electronic absorption spectra and FTIR spectra respectively. The purity of the powder compounds was determined by powder X-ray diffraction (PXRD) patterns using a Rigaku MiniFlex II desktop X-ray diffractometer (30 kV, 15 mA) using Cu-K$_\alpha$ radiation (λ = 1.5418 Å) within 5–50° (2θ) angular range and a fixed-time counting of 4 s at 25 °C. A Bruker esquire 3000 plus mass spectrometer was employed to collect the electrospray ionization (ESI) high resolution mass spectra of the three compounds. CHI 1120A electrochemical analyzer was used for cyclic voltammetric measurements. Electrochemical measurements were performed at 25°C in MeOH in one compartment cell with platinum as working electrode, Pt wire as counter electrode and Ag/AgCl as reference electrode. Electron paramagnetic resonance (EPR) spectra were recorded at 9.13 GHz (X-band) in continuous wave mode with a Bruker ELEXSYS 580 X-band EPR spectrometer equipped with a standard accessory for room temperature operation (298 K). Direct current (dc) magnetic measurements were performed on polycrystalline samples of compounds **2-4** using a Quantum Design SQUID magnetometer equipped with a 5 T magnet. The dc measurements were carried out under an applied field of 0.1 T. Data were corrected for the diamagnetism of the compounds and for the diamagnetic contributions of the sample holder through measurements.

Crystal Data Collection and Refinement

Appropriate single crystals of **3** and **4** were chosen for data collection on a Bruker SMART APEX-II CCD X-ray diffractometer furnished with a graphite-monochromated Mo Kα (λ = 0.71073 Å) radiation by the ω scan (width of 0.3° frame^{-1}) method at 293 K with a scan rate of 5 s per frame. SAINT and XPREP softwares[17] were used for data processing and space group determination. Direct method technique from SHELXS-2014[18] were used for structure determination and then refined by full-matrix least squares technique using SHELXL (2014/7)[19] program package within WINGX version 1.80.05.[20] Data were corrected for Lorentz and polarization effects; an empirical absorption correction was applied using the SADABS.[21] For complex **1** and **2**, the data were collected at 295 K using a Nonius Kappa CCD diffractometer. The dataset was integrated using the Denzo SMN package[22] and corrected for Lorentz, polarization and absorption effects (SORTAV).[23] The structure was solved by direct methods (SIR97)[24] and the calculations were performed using SHELXL-

2014/6[19] and PARST[25] implemented in WINGX suite of programs.[26] The locations of the heaviest atoms (Cu) were determined easily, and the O, N, and C atoms were subsequently determined from the difference Fourier maps. These atoms are refined anisotropically. The H atoms were incorporated at calculated positions and refined with fixed geometry and riding thermal parameters with respect to their carrier atoms. Crystallographic diagrams were presented using DIAMOND software.[27] A summary of the crystal data and relevant refinement parameters is summarized in Table 1. Crystallographic data (including structure factors) have been deposited with the Cambridge Crystallographic Data Centre as supplementary publications CCDC-1857609, 1857607, 1857608 and 1857610. These data can also be obtained free of charge at www.ccdc.cam.ac.uk/conts/retrieving.html (or from the Cambridge Crystallographic Data Centre).

Table 1 Crystal data and structure refinement details for **1-4**

parameters	1	2	3	4
Formula	$C_{72}H_{80}Cu_6N_6O_{40}Cl_6$	$C_{38}H_{34}Cu_4N_4O_{11}F_{12}$	$C_{58}H_{56}Cu_4N_4O_{12}$	$C_{82}H_{121}Cl_3Cu_{10}N_8O_{45}$
F.W. (g mol^{-1})	2263.36	1204.85	1255.26	2680.61
crystal system	Triclinic	Tetragonal	Monoclinic	Triclinic
space group	$P\bar{1}$	$I4_1/a$	$P2_1/c$	$P\bar{1}$
Crystal color	Green	Green	Green	Green
Crystal size/mm^3	0.38×0.26×0.17	0.43×0.34× 0.24	0.38×0.28×0.17	0.30×0.21×0.12
a/ Å	12.3517(4)	12.5200(5)	16.529(3)	14.3300(17)
b/ Å	14.1130(5)	12.5200(5)	22.599(4)	15.8481(19)
c/ Å	14.4440(5)	35.8306(8)	14.645(3)	24.442(3)
α/ deg	77.244(2)	90	90.00	79.731(4)
β/ deg	75.5060(19)	90	99.695(5)	80.665(4)
γ / deg	71.192(2)	90	90.00	83.118(4)
V/ Å^3	2280.45(14)	5616.5(5)	5392.3(18)	5365.8(11)
Z	1	4	4	2
D_c/g cm^{-3}	1.648	1.425	1.543	1.659
μ (mm^{-1})	1.642	1.583	1.624	2.105
F(000)	1150	2408	2568	2740
T/K	295	295	293	295
Total reflns	29155	16627	57121	63654
R(int)	0.0394	0.0538	0.1299	0.0658
Unique reflns	8399	3058	8446	19615
Observed reflns	5928	2200	5764	12878
Parameters	574	184	734	1335

R_1; wR_2 ($I > 2\sigma(I)$)	0.0760, 0.2567	0.0431, 0.1347	0.0977, 0.2210	0.0650, 0.1848
GOF (F^2)	1.065	0.991	1.162	1.024
Largest diff peak and hole (e Å^{-3})	1.546, -0.719	0.425, -0.251	1.243, -0.796	1.452, -0.756
CCDC No.	1857609	1857607	1857608	1857610

$$R_1 = \Sigma(\ ||F_o|-|F_c||\ )/\Sigma|F_o|.\ wR_2 = [\ \Sigma w(|F_o|-|F_c|)^2/\Sigma w(F_o)^2]^{1/2}.\ w = 0.75/(\sigma^2(F_o) +0.0010F_o^2)$$

Kinetic Experiments for Catalytic Oxidation of 3,5-DTBCH$_2$

3,5-di-*tert*-butylcatechol (3,5-DTBCH$_2$) is widely used as a substrate to study its catalytic oxidation and the oxidized product 3,5-di-*tert*-butylquinone (3,5-DTBQ) can be monitored by Uv–*vis* spectroscopy (Shimadzu UV 3100 UV–Vis–NIR spectrophotometer) for appearance of the characteristic band at 390 nm and reproducibility of the reactions were checked three times. With the progress of the oxidation reaction *i.e.,* oxidation of 3,5-DTBCH$_2$ to 3,5-DTBQ, a characteristic and intense absorption band was observed in 300-400 nm range. MeOH solutions of the complexes (~1 × 10^{-5} M) were separately reacted with incremental amounts of the substrate 3,5-DTBCH$_2$ (10 to 100 equivalents) at room temperature under aerobic condition. Ten minutes interval of time scan of reactions for all the complex-substrate combinations was allowed and the data were treated following the initial rate method. The slope of the absorbance versus time plot was used to find the rate of the reaction. Following the Michaelis-Menten equation, a kinetic analysis was performed, and the resultant kinetic parameters were extracted from the double-reciprocal Lineweaver-Burk plots for **1**, **3** and **4**. A modified rate equation (eqn. 7) was used to fit the data for **2** and extract the kinetic parameters.

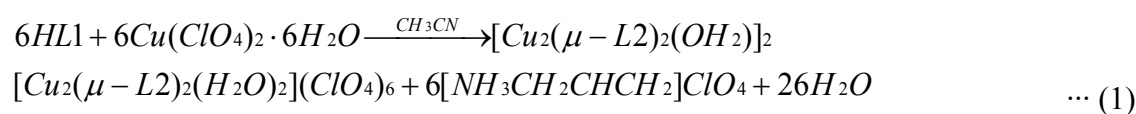## Detection of H$_2$O$_2$ in Catalytic Reaction Medium

Generation of hydrogen peroxide in solution during the catalytic oxidation of DTBCH$_2$ was spectrophotometrically detected following a modified iodometric method.[28] The reaction mixtures were obtained in a similar way as used in the kinetic experiments. The reaction mixture was acidified with H$_2$SO$_4$ (1×10^{-3} M) to *pH* 2 after 1 h to completely quench the reaction. The quinone formed in the reaction medium was extracted three times with CH$_2$Cl$_2$ and then 1 mL of 10% aqueous KI solution was added to the aqueous layer thus obtained. Ammonium molybdate (3%) solution was added in a catalytic amount (3 drops) to accelerate triiodide (I$_3^-$) formation in the presence of H$_2$O$_2$.[28] The reaction that occurs in the medium is H$_2$O$_2$ + 2I$^-$ + 2H$^+$ → 2H$_2$O + I$_2$, and I$_2$ liberated from the reaction combines with an excess iodide ion present in the reaction mixture to form I$_3^-$ ions through I$_2$(aq) + I$^-$ → I$_3^-$. The

H_2O_2 liberated from the reaction mixture was detected by monitoring the band at 353 nm (ε = 26000 L mol^{-1} cm^{-1}), characteristic for I_3^-. A blank experiment (without 3,5-DTBCH$_2$ or without catalyst) was also carried out to check the oxidizing propensity of atmospheric O_2 toward I^-.
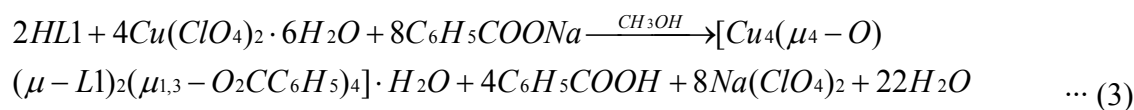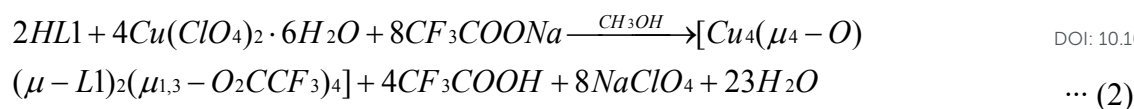
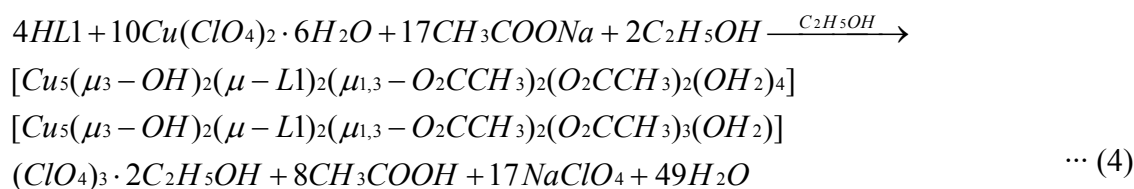## Results and Discussion

Synthesis

Coordination of HL1 to copper(II) ions and the aggregation flexibility of the initially formed species was explored in the absence and presence of different carboxylate ions. Ligand HL1 was synthesized in MeOH by Schiff base condensation of 2,6-diformyl-4-methyl phenol and allylamine in 1:2 molar ratio (Scheme S1). Treatment of HL1 with Cu(ClO$_4$)$_2$·6H$_2$O in MeCN, under aerobic conditions, led to the formation of **1**. On the other hand, reactions of HL1 with Cu(ClO$_4$)$_2$·6H$_2$O in presence of different RCO$_2$Na salts (R = −CF$_3$, −C$_6$H$_5$, −CH$_3$) in MeOH and EtOH, result in the formation of **2**, **3** and **4**, respectively (Scheme 2). Several attempts have been made in other solvents and varying reagent ratios to establish these standardized procedures. Reaction of Cu(ClO$_4$)$_2$·6H$_2$O with HL1 in MeCN in a 1:1 molar ratio in the absence of any base under stirring followed by refluxing conditions, afforded a green solution, from which **1** was isolated as a green block shaped crystal in 54% yield. Use of Cu(ClO$_4$)$_2$·6H$_2$O without added base made the reaction medium slightly acidic (*pH* 5-6), resulting in partial hydrolysis of one ligand imine arm and conversion of L1$^-$ to L2$^-$ as Cu^{II}-bound forms. During this hydrolysis process one Cu^{II} ion and one free allylamine is also eliminated at the beginning. Thus the formation of **1** can be summarized in equation 1.

$$6HL1 + 6Cu(ClO_4)_2 \cdot 6H_2O \xrightarrow{CH_3CN} [Cu_2(\mu - L2)_2(OH_2)]_2$$
$$[Cu_2(\mu - L2)_2(H_2O)_2](ClO_4)_6 + 6[NH_3CH_2CHCH_2]ClO_4 + 26H_2O \qquad \cdots (1)$$

On the other hand, addition of NaO$_2$CCF$_3$ to a mixture of Cu(ClO$_4$)$_2$·6H$_2$O and HL1 in MeOH, in a 4:2:1 molar ratio gave a green solution under stirring, from which **2** can be isolated as green block-shaped crystals in 59% yield. The CF$_3$CO$_2^-$ anions now serve dual roles by modifying the *pH* of the reaction medium to prevent ligand arm hydrolysis and function as linker between two adjacent Cu^{II} centers. In MeOH, the use of NaO$_2$CC$_6$H$_5$ in place of NaO$_2$CCF$_3$ in the same molar ratio resulted in **3** as green block-shaped crystals in 54% yield. Generation of **2** and **3** from these two reactions can be summarized in equation 2 and 3.

$$2HL1 + 4Cu(ClO_4)_2 \cdot 6H_2O + 8CF_3COONa \xrightarrow{CH_3OH} [Cu_4(\mu_4 - O)$$
$$(\mu - L1)_2(\mu_{1,3} - O_2CCF_3)_4] + 4CF_3COOH + 8NaClO_4 + 23H_2O \qquad \cdots (2)$$

$$2HL1 + 4Cu(ClO_4)_2 \cdot 6H_2O + 8C_6H_5COONa \xrightarrow{CH_3OH} [Cu_4(\mu_4 - O)$$
$$(\mu - L1)_2(\mu_{1,3} - O_2CC_6H_5)_4] \cdot H_2O + 4C_6H_5COOH + 8Na(ClO_4)_2 + 22H_2O \qquad \cdots (3)$$

The use of the third type of carboxylate salt as NaOAc in MeOH (molar ratio 4:2:1 for NaOAc:Cu(ClO$_4$)$_2$·6H$_2$O:HL1) reaction medium did not yield any μ_4-oxido-bridged [Cu$_4$] complexes as obtained in equation 2 and 3. Trial reactions using different stoichiometry and solvents such as 4.25:2.5:1 in EtOH on the other hand gave a green solution under stirring condition at room temperature, from which green crystals of **4** were isolated. The formation of **4** can be rationalized by equation 4.

$$4HL1 + 10Cu(ClO_4)_2 \cdot 6H_2O + 17CH_3COONa + 2C_2H_5OH \xrightarrow{C_2H_5OH}$$
$$[Cu_5(\mu_3 - OH)_2(\mu - L1)_2(\mu_{1,3} - O_2CCH_3)_2(O_2CCH_3)_2(OH_2)_4]$$
$$[Cu_5(\mu_3 - OH)_2(\mu - L1)_2(\mu_{1,3} - O_2CCH_3)_2(O_2CCH_3)_3(OH_2)]$$
$$(ClO_4)_3 \cdot 2C_2H_5OH + 8CH_3COOH + 17NaClO_4 + 49H_2O \qquad \cdots (4)$$

Use of NEt$_3$, NaOMe or NaOH bases resulted only intractable green gummy masses, which were not suitable for further characterization and crystallization.
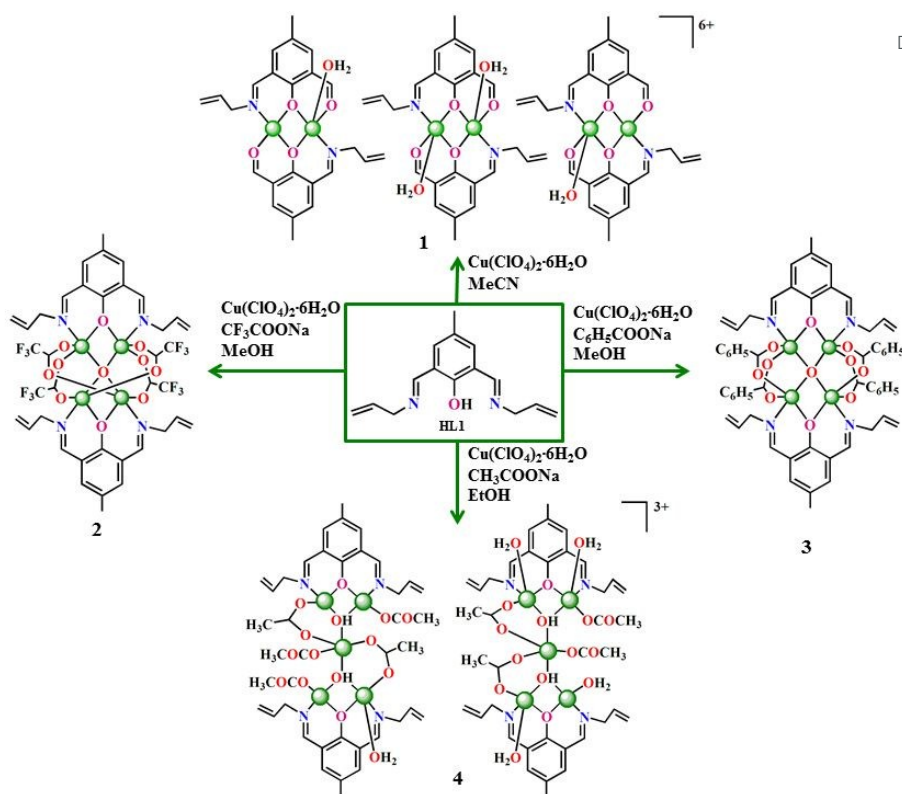
Scheme 2 Synthetic routes for **1-4**

Characterization. FTIR Spectra

Initial solid state characterization of the isolated reaction products were carried out using IR spectroscopy to pinpoint the presence of the parent ligand system and carboxylates. It established the binding of L1⁻ to Cu^{II} centers in **2**, **3** and **4** and L2⁻ to Cu^{II} centers in **1** (Figure S1). The presence of Cu^{II}-bound water molecules in **1**, crystal lattice water molecule in **3**, and Cu^{II}-bridged OH⁻ groups, coordinated and lattice water molecules in **4** are manifested by single broad and medium intensity IR bands at 3478, 3447 and 3447 cm^{-1} respectively. The characteristic Cu^{II}-bound $\bar{\nu}_{C=N}$ stretching frequencies from the ligand backbone appeared at 1636, 1624, 1636 cm^{-1} for **2**, **3**, **4** respectively and at 1629 cm^{-1} for **1**. The lattice ClO$_4^{-}$ ions (in T_d site symmetry) in **1** showed a strong band at 1104 cm^{-1} for $\nu_3(T_2)(\nu_{ClO})$ and a medium intense one at 622 cm^{-1} for the $\nu_4(T_2)(\delta_{dOClO})$ modes.[29] For **2** and **3** the presence of bridging trifluoroacetates and benzoates were confirmed at 1688, 1436 and 1611, 1458 cm^{-1}, respectively for the asymmetric ($\bar{\nu}_{as(COO)}$) and symmetric ($\bar{\nu}_{s(COO)}$) stretching vibrations. The differences ($\Delta\bar{\nu}$ = 252 cm^{-1}, and 153 cm^{-1}) in these two values were characteristic for $\mu_{1,3}$−bridging modes of four CF$_3$COO⁻ in **2** and four C$_6$H$_5$COO⁻ bridges in **3**. In the case of

CF_3COO^- bridging, the asymmetric stretching vibration occurred at higher frequency due to the attachment of electron-withdrawing fluorine atoms.[30] For **4**, the asymmetric and symmetric stretching vibrations are detected at 1564 cm^{-1} ($\bar{v}_{as(COO)}$) and 1412, 1338 cm^{-1} ($\bar{v}_{s(COO)}$) for $\mu_{1,3}$-bridging type and monodentate coordination. The $\Delta\bar{v}$ = 152 cm^{-1} thus confirmed the former type and $\Delta\bar{v}$ = 226 cm^{-1} was for the latter type.[31] The presence of anionic ClO_4^- groups (in T_d site symmetry) in **4** is indicated by a broad Cl−O stretching mode at 1092 cm^{-1} characteristic for $v_3(T_2)(v_{ClO})$ stretching and a medium intensity vibration for Cl−O bending at 623 cm^{-1} due to $v_4(T_2)(\delta_{dOClO})$ mode.[8]

Powder X-ray Diffraction Patterns

The powder XRD patterns for the bulk materials of **1-4** were recorded using a Bruker AXS X-ray diffractometer and compared with the simulated ones derived from the single crystal X-ray diffraction data. Figure S2 shows good agreement of the experimentally obtained powder patterns to that of the simulated ones. The difference in intensity in some 2θ values is due to the different orientations of the crystallites in the powder samples. From the sharpness of the peaks and the correspondence with simulated patterns we conclude that the powder samples are crystalline and phase pure with the absence of extra peaks for impurities.

Electronic Spectra

Electronic transitions for **1**–**4** in MeOH solution in the 200-800 nm range exhibit representative absorption bands for each aggregate. The ligand-field absorption bands (λ), with maxima at 708 nm (ε = 76 L mol^{-1} cm^{-1}), 666 nm (ε = 104 L mol^{-1} cm^{-1}), 635 nm (ε = 184 L mol^{-1} cm^{-1}) and 670 nm (ε = 157 L mol^{-1} cm^{-1}), were found for **1**, **2**, **3** and **4** respectively. The higher energy bands due to the ligand-to-metal charge transfer (LMCT) transitions within the metal ion bound ligand fragment were observed at 366 nm (ε = 19300 L mol^{-1} cm^{-1}), 372 nm (ε = 8100 L mol^{-1} cm^{-1}), 366 nm (ε = 16400 L mol^{-1} cm^{-1}) and 367 nm (ε = 48300 L mol^{-1} cm^{-1}) respectively. Quite intense absorptions at 243 nm (ε = 91600 L mol^{-1} cm^{-1}), 261 nm (ε = 45400 L mol^{-1} cm^{-1}), 259 nm (ε = 91100 L mol^{-1} cm^{-1}) and 258 nm (ε = 238800 L mol^{-1} cm^{-1}) were dominated by the metal ion bound ligand-based $\pi\rightarrow\pi^*$ (LLCT) transitions (Figure S3).

EPR Spectra

Powdered samples of **1-4** were also characterized by recording their X-band EPR spectra at 298 K. They show representative *axial* signals at g ~ 2.0 for Cu^{II} centers (Figure S4).[32] Weak

and forbidden transitions at the half field of the $g \sim 2.0$ signal ($\Delta M_S = \pm 2$ transitions) were observed at 1605 G ($g = 4.29$), 1613 G ($g = 4.25$), 1607 G ($g = 4.28$) and 1607 G ($g = 4.28$) for complexes **1-4** respectively indicating the presence of spin-spin interactions.[32] For complexes **1** and **2** definite $g_\parallel$ and $A_\parallel$ values could not be determined due to poor resolution of split patterns of the parallel component. The $g_\perp$ signals were found at 2.13 and 2.11 with hyperfine splitting in this region and corresponding $A_\perp = 83.19 \times 10^{-4}$ cm^{-1}, 81.63×10^{-4} cm^{-1} respectively. On the other hand complex **3** and **4** gave $g_\parallel = 2.27$ and 2.25, and $g_\perp = 2.08$ and 2.10 respectively. In this case the average hyperfine constants were $A_\parallel = 159.85 \times 10^{-4}$ cm^{-1}, 150.50×10^{-4} cm^{-1} and $A_\perp = 75.40 \times 10^{-4}$ cm^{-1}, 81.01×10^{-4} cm^{-1} respectively.

Description of Crystal Structures

$[Cu_2(\mu–L2)_2(H_2O)]_2[Cu_2(\mu–L2)_2(H_2O)_2](ClO_4)_6$ (1). A green block-shaped single crystal of **1**, obtained by slow evaporation of a MeCN solution, was used to find the molecular structure. Complex **1** crystallized in triclinic $P\bar{1}$ space group. Important bond distances and angles are summarized in Table S1. Two of the anionic hydrolyzed ligands (L2$^-$), providing central phenoxido groups, were utilized to trap two Cu^{II} centers in a centro-symmetric manner resulting in Cu$_2$O$_2$ motif. In two cases the coordination geometry around Cu^{II} were different, *square planar* (Cu1 and Cu1*) and *square pyramidal* (Cu2 and Cu2*). For the central species both the Cu^{II} (Cu3 and Cu3*) centers have *square-pyramidal* coordination geometry. Within the *basal* planes the Cu–O and Cu–N distances from aldehyde O and imine N are close, *e.g.*, Cu1−O4, 1.940(5) Å; Cu2–O2, 1.943(4) Å and Cu1–N1, 1.937(5) Å; Cu2−N2, 1.940(5) Å. Interestingly the bridging phenoxido functions also display similar bond lengths *e.g.*, Cu1−O1, 1.936(4) Å; Cu1−O3, 1.944(4) Å; Cu2−O1, 1.959(4) Å; Cu2−O3, 1.945(4) Å (Figure 1). The *apical* water (O1W and O2W) molecules showed longer Cu–O distances at 2.300(5) and 2.291(5) Å. Within the Cu$_2$O$_2$ motif the Cu···Cu separations are 3.0163(9) and 3.0307(12) Å and the Cu–O–Cu angles are at 101.51(17)–101.71(17)° range and 101.63(18)º for two types of [Cu$_2$] units.[33]
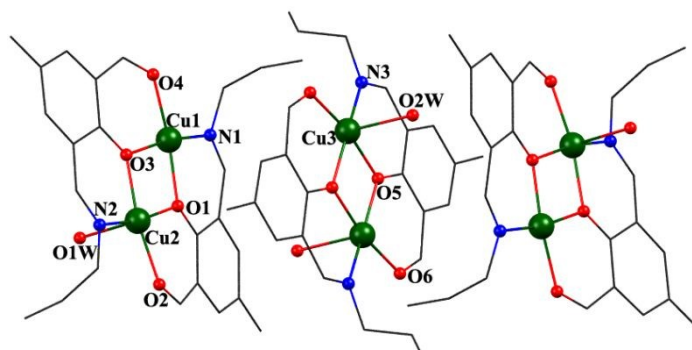
Dalton Transactions

Figure 1 Structural view of **1** with partial atom numbering scheme. H atoms are omitted for clarity. Colour code: Cu, green; N, blue; O, red; C, black

$[Cu_4(\mu_4-O)(\mu-L1)_2(\mu_{1,3}-O_2CCF_3)_4]$ (2). With $Z = 4$ compound **2** crystallizes in the tetragonal $I4_1/a$ space group. Selected metric parameters are summarized in Table S1. The tetranuclear structure of **2** is shown in Figure 2a. Two capping N_2O donor set bearing $L1^-$ parts bind two Cu^{II} centers to give $\{Cu_2(OH)\}$ fragments. Two such fragments in the next step assemble around a central μ_4-O group to provide the *tetrahedral* $\{Cu_4O\}$ core. Bridging by four trifluoroacetate and two phenoxido groups complete the Cu···Cu links on six faces of the cube (Figure 3a). The phenoxido-bridged faces record shorter Cu··Cu separations at 2.9979(6) Å and the clipping by trifluoroacetate groups register longer intermetallic separations at 3.2231(1) Å. ~~Each~~ The Cu^{II} center remains in a *square-pyramidal* O_4N coordination environment (Addison $\tau_5 = 0.12$)[34], where the shortest distance (Cu−O, 1.9290(3) Å) was provided by the O-atom of the μ_4-oxido group and the *apical* coordination from trifluroacetato O-atom give Cu−O distance of 2.342(3) Å (Figure 2b and 2c). Three possible carboxylate coordination modes for bridging two adjacent metal ion centers are known. These are *syn-syn*, *syn-anti* and *anti-anti* bridging modes. The distorted *syn-syn* coordination from four bridging carboxylates in $\mu_{1,3}$-mode was responsible for placing one *syn* O-atom of carboxylate anion at the *basal* site of one copper center and another distorted *syn* O-atom of the same carboxylate anion at the *apical* site of another copper center for complementary *basal-apical* clipping (Figure 3b). The *basal* Cu−O bond (1.962(2) Å) is shorter compared to the apical one (2.342(3) Å). The amount of twisting of carboxylate anions for distorted *syn-syn* coordination can be estimated from the C−C−O−Cu/C−C−O−Cu torsion angles (179.59/141.85°).
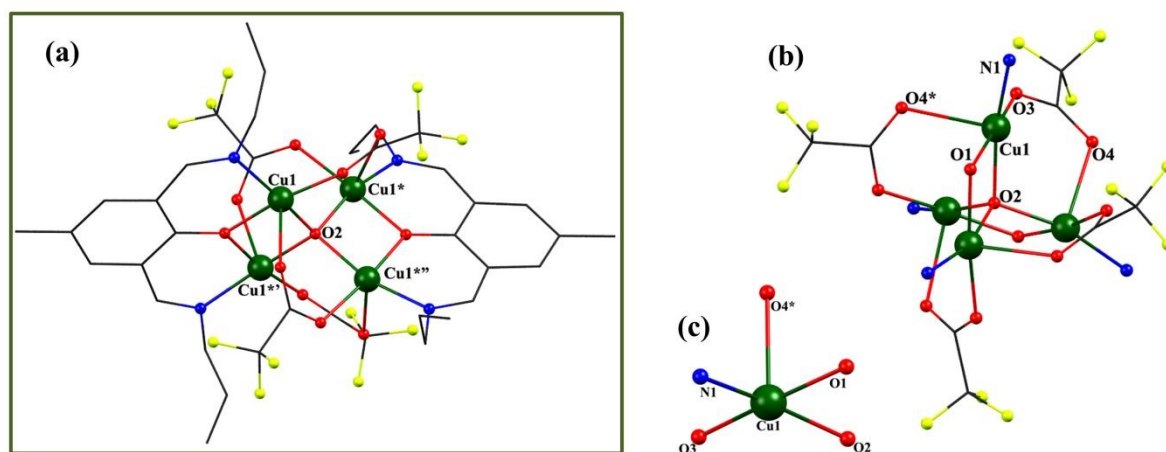
Figure 2 (a) Structural view of **2** with partial atom numbering scheme. H atoms are omitted for clarity; (b) Atom connectivity within [Cu$_4$] core; (c) Coordination environment around each Cu center. Colour code: Cu, green; N, blue; O, red; C, black; F, yellow
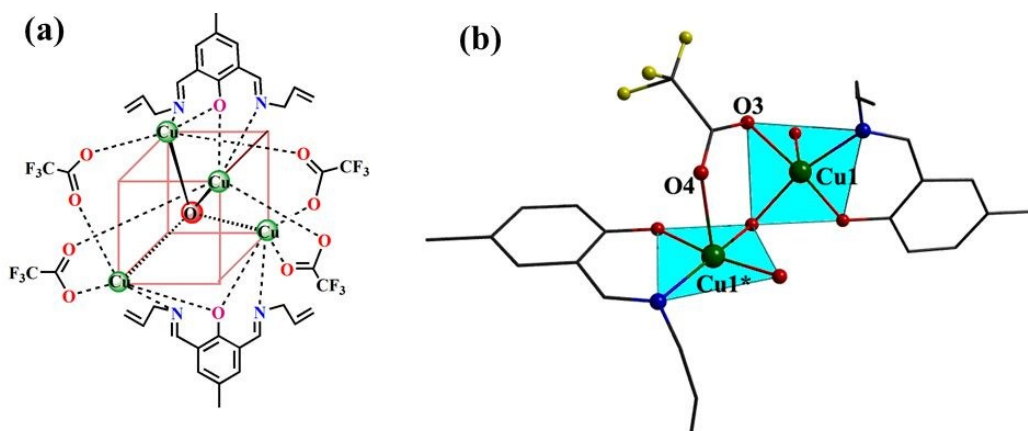

Figure 3 (a) Trifluoroacetato connectivity in **2**; (b) Distorted *syn-syn* coordination of each trifluroacetate groups for complementary *basal-apical* coordination

Careful checking of the crystal packing arrangements revealed no hydrogen bonding network or CH$\cdots\pi$ interactions to be present in **2**.

[Cu$_4$(μ_4-O)(μ-L1)$_2$($\mu_{1,3}$–O$_2$CC$_6$H$_5$)$_4$]·H$_2$O (3). Compound **3** crystallizes in the monoclinic *P*2$_1$/*c* space group with *Z* = 4 and the asymmetric unit has one [Cu$_4$] unit and a lattice water molecule. The structure is shown in Figure 4a and important bond lengths and angles are listed in Table S1 in Supporting Information.
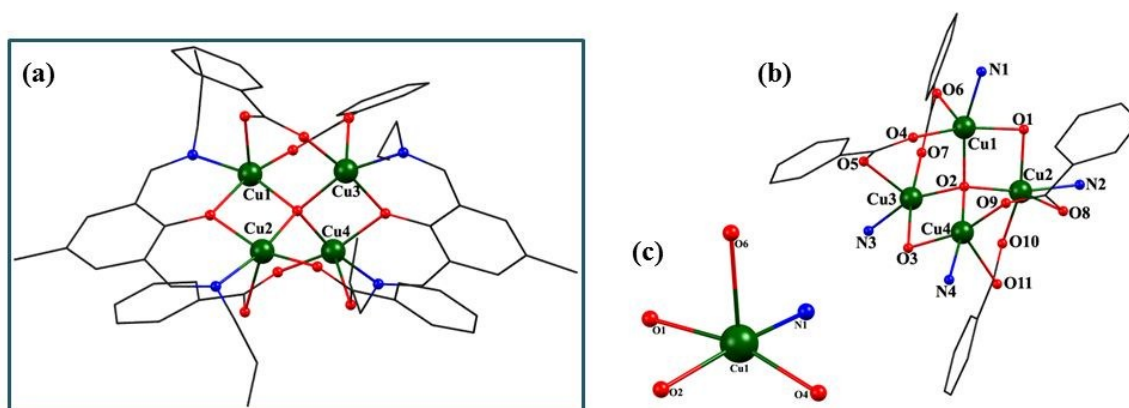

Figure 4 (a) Structural view of **3** with partial atom numbering scheme and H atoms are omitted for clarity; (b) Atom connectivity within [Cu$_4$] tetrahedron; (c) Representative coordination geometry around each Cu^{II} centre. Colour code: Cu, green; N, blue; O, red; C, black

Unlike the previous case, the nature of bridging of four benzoate groups were different. Now two of the cube faces were spanned by two benzoates leading to intermediate Cu$\cdots$Cu separations of 3.193(2) and 3.082(2) Å. The other two faces where no clipping groups were

present the Cu···Cu distances were longest at 3.204 and 3.286(2) Å (Figure 5a). Similar to the previous case Cu···Cu separations in L1⁻ bridged faces are the smallest (3.021(2) and 3.0105(18) Å). Herein all four Cu^II centers showed varying Addison τ_5 values (Cu1 = 0.03, Cu2 = 0.13, Cu3 = 0.22 and Cu4 = 0.08). The distorted *syn-syn* coordination modes of two benzoates to Cu1-Cu3 and Cu2-Cu4 brought the *syn* O-atom to the *basal* site and another *syn* O-atom to the *apical* site of Cu^II centers in a regular and complementary fashion (Figure 5b). For all the metallic sites the *basal* Cu−O bonds were shorter at 1.930(7) Å – 1.964(7) Å compared to the apical ones at 2.214(9) Å – 2.397(7) Å (Figure 4b and 4c).
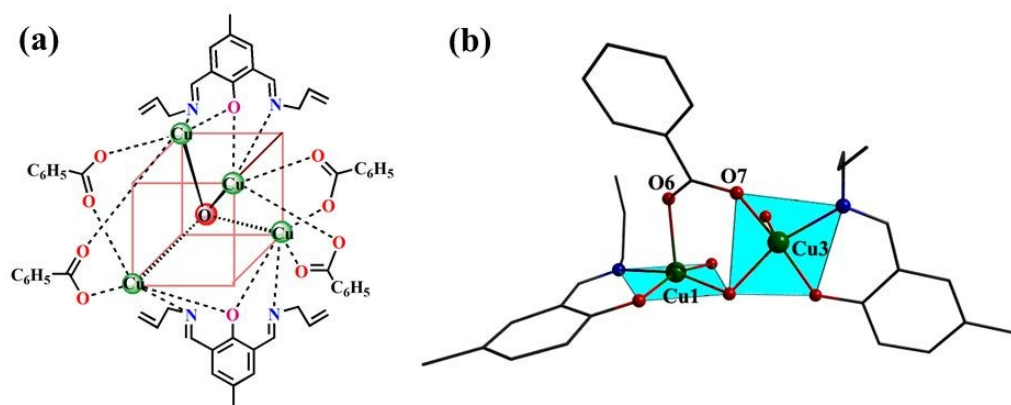
Figure 5 (a) Benzoato connectivity in **3**; (b) Complementary *basal-apical* clipping by benzoate groups.

[Cu₅(μ₃-OH)₂(μ-L1)₂(μ₁,₃−OAc)₂(OAc)₂(H₂O)₄][Cu₅(μ₃-OH)₂(μ-L1)₂(μ₁,₃−OAc)₂(OAc)₃(H₂O)](ClO₄)₃·2C₂H₅OH (4). Compound **4** forms green crystals in the triclinic *P* $\overline{1}$ space group and the structural view is presented in Figure 6. The unit cell of this compound is very much similar to the copper-based shattuckite mineral and consists of two [Cu₅] units, three perchlorate anions, and two lattice EtOH molecules. Important bond lengths and angles are listed in Table S1. The pentanuclear Cu^II-based aggregate was formed by trapping of a central Cu^II center by two ligand bound {Cu₂(OH)} fragments which were instrumental to give **2** and **3** by a direct assembling process. In these two cases, condensation of two bridging hydroxido groups result a central μ₄−O group (2HO⁻ → H₂O + O²⁻), necessary for the formation of {Cu₄O} core. In the case of **4** two of these hydroxido bridges have the control on the generation of two [Cu₅] entities as is known in the case of copper-based minerals shattuckite, Cu₅(OH)₂(SiO₃)₄, cornubite, Cu₅(OH)₄(AsO₄)₂ and with chlorido in place of the hydroxido group in Cu₅Cl₂(SeO₃)₄.[35,36] Two slightly different [Cu₅] coordination units, having two or one positive charges, were present within one unit cell. In these two cases the bridging network between the five Cu^II ions are ensured by two water derived μ-HO⁻ ions,

two μ$_{1,3}$ acetato bridges, terminal acetates and two μ-phenoxido fragments from deprotonated L1$^-$ ligands.
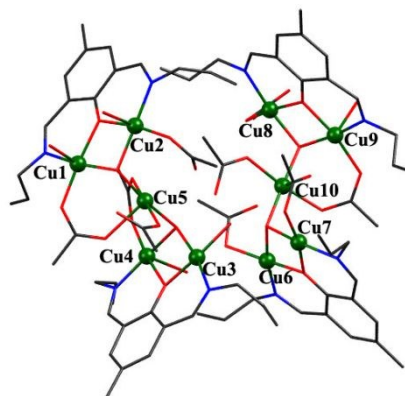

Figure 6 POV-ray view of the two parts in **4** with atom numbering scheme. Hydrogen atoms are omitted for clarity. Color code: Cu, green; N, blue; O, red; C, black

In both the two cases the central Cu^{II} centers remained in distorted *square-pyramidal* (τ$_5$ = 0.05) coordination geometry having five O-donor atoms from the coordination of two hydroxido O centers in *basal* sites and, two acetato groups in μ$_{1,3}$ mode and one as monodentate. The O atoms of bridging acetato group were responsible for long Cu–O *apical* bonds as expected from a Jahn-Teller distortion (Figure 7). After establishing the acetato coordination network and depending upon the preference for coordination geometries and availability of coordination sites, water molecules were coordinated to some Cu^{II} centers. Two [Cu$_5$] coordination units have two types of acetato coordination networks within **4** (Figure 6). In the first part (dicationic unit), including the central one, four Cu^{II} centers are in *square pyramidal* (τ$_5$ values 0.11, 0.08, 0.03 and 0.05) geometry and Cu3 in *square planar* (τ$_4$ = 0.17) geometry having unusual coordination of one H$_2$O (Figure 7). Within the two L1$^-$ bridged part the Cu···Cu separations are 3.0442(12) and 3.0396(13) Å.
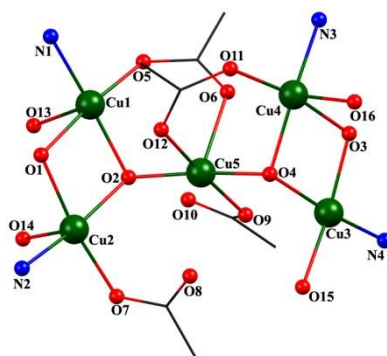

Figure 7 View of cationic pentametallic core of first part of **4**

In the second part the number of acetato groups and their connectivity pattern were different. Now three centers in *square planar* (τ_4 = 0.16, 0.17 and 0.16) geometry, while remaining two in *square pyramidal* (τ_5 = 0.01 and 0.10) geometry (Figure 8). Within the two L1$^-$ bridged part the Cu$\cdots$Cu separation is 3.0401(13) Å for *square pyramidal-square planar* centers and 3.0007(13) Å for two in *square planar* geometry.
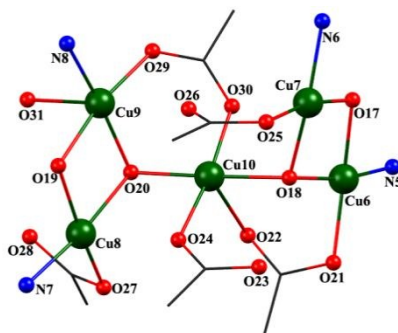

Figure 8 View of cationic pentametallic core of second part of **4**

Both the two [Cu$_5$] parts were more open and distorted compared to other known arrangements based on vertex-shared open-dicubanes.[10]

Magnetic Measurements

The magnetic properties of complexes **2**, **3** and **4** were investigated by direct current (dc) magnetic susceptibility measurements on powdered samples under an applied field of 0.1 Tesla and are plotted as $\chi_M T$ *vs.* *T* in Figure 9. For **1**, **2** and **3** the magnetic susceptibility measurements were difficult. In particular for **1** the magnetic susceptibility signal was extremely low at room temperature, indicative of strong antiferromagnetic interactions between the two Cu^{II} centers suggesting a very well-isolated singlet spin ground state (*S*=0) and no further measurements were undertaken. For **2** and **3** the signal becomes extremely low below 110 K and 50 K, respectively. Complex **4**, [Cu$^{II}_5$], presents better behavior and a complete measurement, from 290 K to 5 K, was possible.
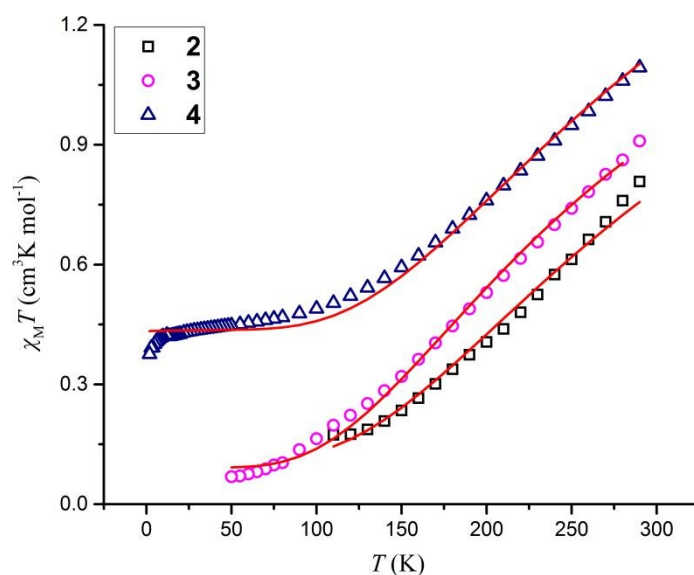
Figure 9 $\chi_M T$ *vs. T* plot for complexes **2–4** under an applied dc field of 0.1 T. The solid lines represent a fit of the data (see the text for details)

The room temperature $\chi_M T$ values of all complexes are significantly lower compared to the theoretical values, indicating that strong dominant antiferromagnetic interactions exist between the Cu^{II} ions; the room temperature $\chi_M T$ values of 0.81 cm^3 K mol^{-1} and 0.91 cm^3 K mol^{-1} for **2** and **3** respectively, are below the expected value of 1.73 cm^3 K mol^{-1} for four non-interacting $S = 1/2$ ions with $g = 2.15$. Upon cooling, $\chi_M T$ decreases reaching a minimum value of 0.17 cm^3 K mol^{-1} at 110 K for **2** and ~ 0.1 cm^3 K mol^{-1} at 50 K for **3**. Below 110 K and 50 K, for **2** and **3** respectively, further measurements were extremely difficult due to the very small signal and subsequent poor signal-to-noise ratio, suggesting a well-isolated singlet spin ground state ($S = 0$) for both the complexes (*vide infra*). For complex **4** the experimental $\chi_M T$ value of 1.10 cm^3 K mol^{-1} at 290 K is lower than the theoretical value of 2.17 cm^3 K mol^{-1} for five non-interacting $S = 1/2$ ions with $g = 2.15$. Upon cooling, $\chi_M T$ decreases reaching a minimum value of 0.38 cm^3 K mol^{-1} at 2 K.

It has been reported previously that in Cu^{II} complexes the magnetic interactions mediated through bridges coordinated on the *basal* plane are stronger than those in the *apical* positions.[37] With this in mind, complexes **2** and **3** can be considered as two phenoxido-oxido-bridged $[Cu^{II}_2]$ units interacting weakly through a central μ_4-oxido bridge.[38] In each $Cu^{...}Cu$ dinuclear unit the metals are bridged through a double μ_4-oxido/ phenoxido bridge, which has been described as a much more efficient interaction compared to the single μ_4-oxido group bridging the two $[Cu^{II}_2]$ units.[11] Using the program PHI[39] we were able to fit the magnetic

susceptibility data for complexes **2** and **3** by adopting a simple 1-*J* model (see Figure 10, left and eqn. 5), which avoids any over parameterization in the fit.

$$\hat{H} = -2J(\hat{S}_1 \cdot \hat{S}_2 + \hat{S}_3 \cdot \hat{S}_4) + g\mu_B \vec{B}\sum_{i=1}^{4} \vec{s}_i \qquad (5)$$
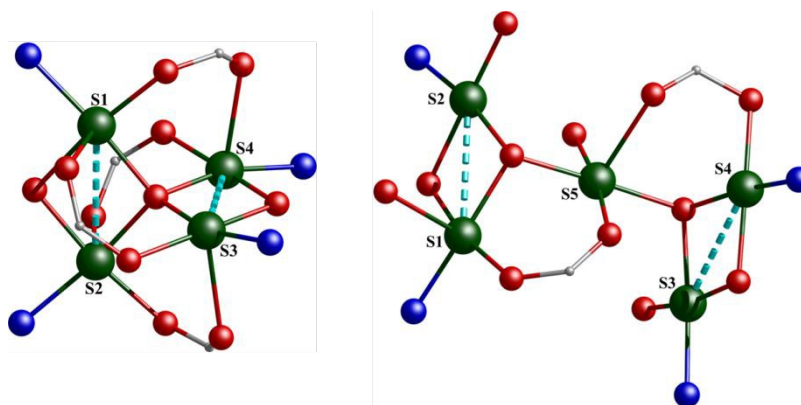

Figure 10 Exchange interaction (*J*) scheme for **2** and **3** (left) and **4** (right). Color code: cyan dashed line = *J*, O = red, Cu = green, N = dark blue, C = grey

The best fit afforded *J* = −204 (±1) cm^{-1} and *J* = −174 (±1) cm^{-1}, for **2** and **3** respectively, with the *g*-value fixed at 2.15. Small *S* = 1/2 spin impurities were also considered for **2** (3.5%) and **3** (2.9%), consistent with those previously reported in similar complexes.[38,11,40,41] The fit results in a singlet ground state (*S* = 0) with the first excited state (*S* = 1) located at ∼ 400 cm^{-1} and ∼ 350 cm^{-1} for **2** and **3**, respectively. The strong antiferromagnetic coupling in **2** and **3** is not uncommon when Cu^{II} ions are bridged through phenoxido groups and the Cu–O$_{phenoxido}$–Cu angle is larger than 97.6°, with the strength of the antiferromagnetic interaction increasing with the angle.[42,43] Given that the Cu–O$_{phenoxido}$–Cu and Cu–O$_{oxido}$–Cu angles are 100.5° and 102° for complex **2** and 98° and 104° for **3**, it is not surprising that the exchange interaction, *J*, through the μ$_4$-oxido/phenoxido bridge is large and antiferromagnetic.

For complex **4**, the data were fitted considering one dominant exchange interaction between the phenoxido-bridged Cu^{II} ions (Figure 10) adopting the approach previously reported for similar complexes, which avoids any overparameterization in the fit.[37,44] Using the program PHI[39] and adopting the Hamiltonian shown in eqn. 6

$$\hat{H} = -2J(\hat{S}_1 \cdot \hat{S}_2 + \hat{S}_3 \cdot \hat{S}_4) + g\mu_B \vec{B}\sum_{i=1}^{5} \vec{s}_i \qquad (6)$$

we were able to simultaneously fit the magnetic susceptibility and magnetization data (Figure 11). The best fit yielded *J* = −205 (±2) cm^{-1} with the *g*-value fixed at 2.15. The fit results in

an $S = 1/2$ ground state with the first excited state located at ~ 400 cm^{-1}. The magnitude and the nature of the exchange interaction is in agreement with previously reported Cu^{II} complexes with similar geometric parameters; the Cu–O$_{phenoxido}$–Cu angles are ~101° (above the critical angle of 97.6°).[42,43]
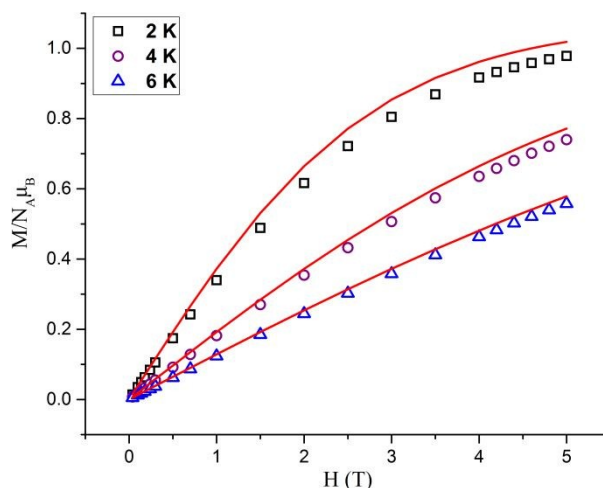
Figure 11 M *vs.* H plot for complex **4** in the 1 – 5 T field range. The solid lines represent the fit of the data (see the text for details)

Catechol Oxidation Activity

In this part of the work, we examined all four complexes for the catechol oxidase model study.[7] Our intention was to reveal the efficacy of the reported compounds of varying nuclearity for any catalytic oxidation of the most widely used model substrate 3,5-di-*tert*-butylcatechol (3,5-DTBCH$_2$) at 298 K in MeOH solutions saturated with O$_2$. Generation of the oxidized quinone product (3,5-DTBQ) was followed by monitoring the increase in absorbance in UV-vis region of the characteristic band of quinone as a function of time. A lower redox potential for this substrate and the presence of bulky substituents for a slower ring opening reaction during any kind of follow-up oxidation prompted us to choose this substrate.[45] To measure the catechol oxidation potential of complexes **1-4**, ~1×10^{-5} mol L^{-1} solutions were treated with a ~1×10^{-3} mol L^{-1} solution of 3,5-DTBCH$_2$ in air for the collection of time-dependent UV-vis spectra up to 50 mins (Figure S5). Treatment of Cu(ClO$_4$)$_2$·6H$_2$O with 3,5-DTBCH$_2$ did not exhibit any change in the absorption intensity, even after 6 h of addition under similar reaction conditions.

Initial rate methods were applied to examine the kinetic behavior of oxidation of 3,5-DTBCH$_2$ by complexes **1-4**, by monitoring the characteristic absorption band for substituted quinone at 390 nm in MeOH as a function of time. A first-order dependence of the rates on substrate concentrations were observed on treating the complexes **1-4** with varying

concentrations of 3,5-DTBCH$_2$. However complexes **1**, **3** and **4** show saturation kinetics at higher 3,5-DTBCH$_2$ concentrations. Thus a Michaelis-Menten model is used for fitting the rates (obtained by initial rate method) for **1**, **3** and **4** (Figure 12) and the kinetic parameters were extracted from the Lineweaver-Burk plots (Figure 12 insets).
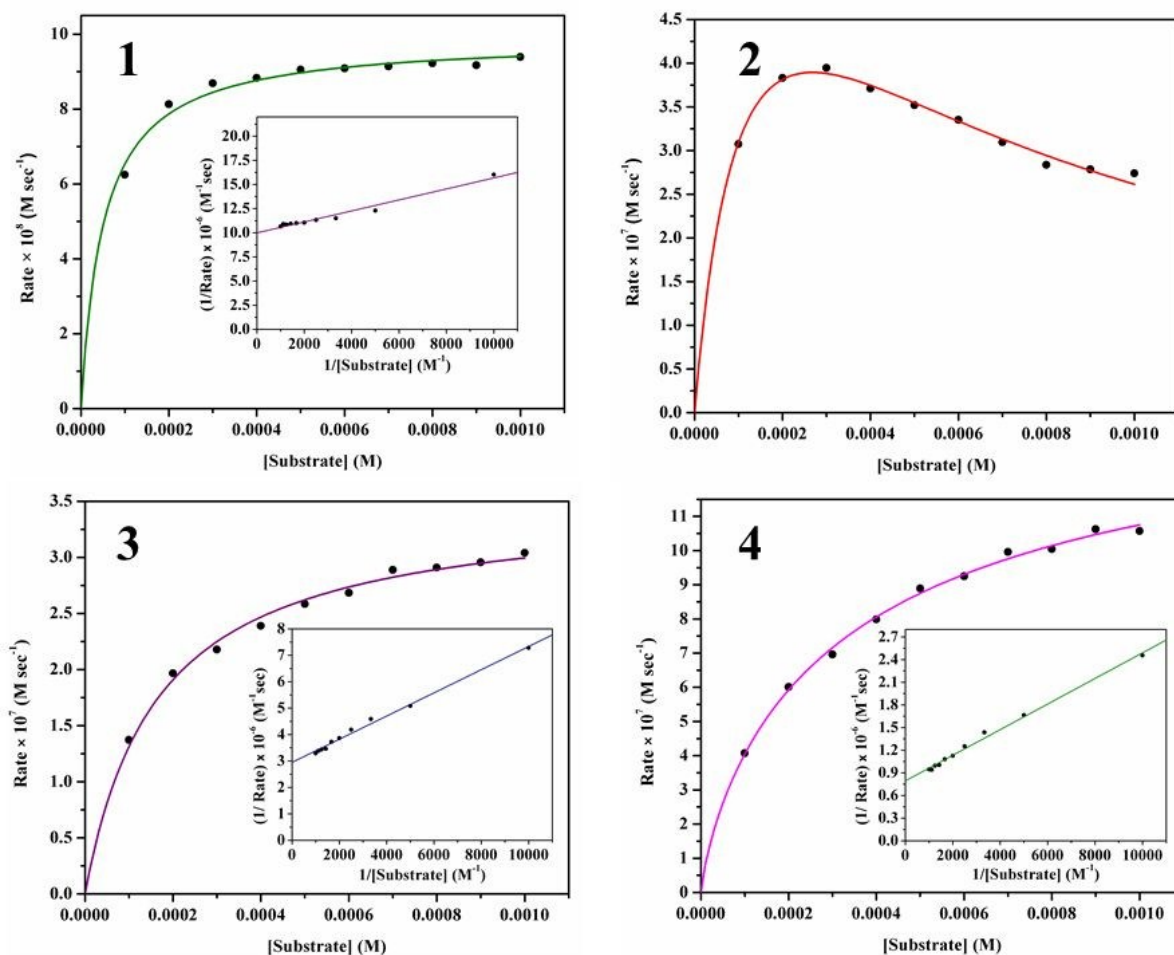

Figure 12 Dependence of the reaction rates on the substrate concentration for the oxidation of 3,5-DTBCH$_2$ catalyzed by complexes **1-4** in MeOH. The Lineweaver−Burk plots (inset)

The binding constant (K_M), the maximum velocity (V_{max}), and the rate constants for the dissociation of the complex-substrate intermediate (*i.e.*, the turnover number, k_{cat}) are obtained from the Lineweaver-Burk plot of $1/V$ vs $1/[S]$. The kinetic parameters V_{max}, K_M, and K_{cat} for **1**, **3** and **4** were collected in Table 2. In case of complex **2**, inhibition by substrate molecules was observed and the reaction rate did not reach a plateau at high substrate concentration as observed in the other three cases (Figure 12). This behavior may be assumed due to the formation of inactive mononuclear species in the presence of excess 3,5-DTBCH$_2$. In the other three cases, the catalytic potency may be explained due to the difference in the availability and nature of catalytically active ligand bound {Cu$_2$} fragments. For **2**, the

decomposition of hydroxido-bridged {Cu$_2$} species in solution limits the possibility of two electron oxidation of 3,5-DTBCH$_2$ to 3,5-DTBQ. In the case of **2** a simple Michaelis-Menten model with the establishment of a pre-equilibrium cannot be used to describe the kinetic process. A modified rate equation was used to fit the rate data as per the mechanism represented in Scheme S2, where K$_c$ is the formation constant of the inactive mononuclear species.[46] Kinetic treatment considering initial rates and a large excess of 3,5-DTBC resulted the following equation.

$$r = \frac{k_{cat}[\text{DTBC}][\text{Cat}]}{K_M\left(1 + K_C[\text{DTBC}]^2\right) + [\text{DTBC}]}...(7)$$

The parameters obtained by applying equation 7 to the data for **2** were listed in Table 2 along with **1**, **3** and **4**

Table 2 Kinetic parameters for the oxidation of 3,5-DTBCH$_2$ by **1-4** in MeOH

Complex	V_{max} (10^{-6} M S^{-1})	K_M (10^{-4} M)	k_{cat} (h^{-1})	k_{cat}/K_M (10^3 M^{-1} h^{-1})	K_C (10^7 M^{-2})
1	0.1001	0.5569	36.045	632	−
2	−	1.2879	274.896	2134.4	1.3911
3	0.3394	1.4883	122.174	820.8	−
4	1.2603	2.1377	453.732	2122.4	−

High Resolution Mass Spectroscopic Evidences for Fragments in Solution

To obtain a reasonable idea about the nature of the various fragments present in solution, possible catalyst–substrate intermediates during oxidation reactions and insight into the mechanism of catalytic cycles, MeOH solutions of complexes **1-4** were examined by HRMS analysis. All four complexes exhibited a common peak at *m/z* value of 243.2511 corresponding to the protonated ligand [HL1-H]$^+$ (C$_{15}$H$_{19}$N$_2$O; Calcd 243.1497) (Figure S6). In the case of **1**, the base peak obtained at *m/z* value of 204.1013 is due to the protonated and hydrolyzed ligand fragment [HL2-H]$^+$ (C$_{12}$H$_{14}$NO$_2$; Calcd 204.1025). The same peak, of lesser intensity, was also present in the solutions of **2-4**.

A medium intensity peak at *m/z* value of 445.1441 for **1** was considered for [(HL2)$_2$-K]$^+$ (C$_{24}$H$_{26}$KN$_2$O$_4$; Calcd 445.1530) and other peaks at 266.0243, 468.1140, 490.0925 and 530.0331 (Figure S6) were assigned to the fragments [Cu(L2)-H]$^+$ (C$_{12}$H$_{13}$CuNO$_2$; Calcd 266.042), [Cu(L2)$_2$-H]$^+$ (C$_{24}$H$_{25}$CuN$_2$O$_4$; Calcd 468.1110), [Cu(L2)$_2$-Na]$^+$ (C$_{24}$H$_{24}$CuN$_2$NaO$_4$; Calcd 490.0930) and [Cu$_2$(L2)$_2$]$^+$ (C$_{24}$H$_{24}$Cu$_2$N$_2$O$_4$; Calcd 530.0323). For the mixture of **1**

and 3,5-DTBCH$_2$ in 1:100 molar ratio in MeOH (Figure S7) after 10 min of mixing the peaks at m/z = 243.1381 and 463.2868 for [3,5-DTBQ-Na]$^+$ and [(3,5-DTBQ)$_2$-Na]$^+$, respectively clearly showed the formation of free quinone in solution. The low intensity peak at 529.2902 is obtained for the catalyst-semiquinonate adduct [Cu$_2$(L2)$_2$(DTSQ)$_2$(CH$_3$OH)$_2$-HNa]$^{2+}$ (C$_{54}$H$_{73}$Cu$_2$N$_2$NaO$_{10}$; Calcd 529.1872) establishing the [Cu$_2$(L2)$_2$]$^+$ fragment as the catalytically active species in solution.

The mass spectrum of **2** shows a peak at m/z = 409.0576 for the dinuclear fragment [Cu$_2$(L1)(OH)(CF$_3$COO)$_3$(CH$_3$OH)-HNaK]$^{2+}$ (C$_{22}$H$_{23}$Cu$_2$F$_9$KN$_2$NaO$_9$; Calcd 408.9688) (Figure S8). Mixture of **2** and 3,5-DTBCH$_2$ in 1:20 molar ratio in MeOH after 10 min of mixing gave peak at 587.1411 for the catalyst-semiquinonate adduct [Cu$_2$(L1)(OH)(CF$_3$COO)$_2$(DTSQ)$_2$-(2Na)(2K)]$^{2+}$ (C$_{47}$H$_{58}$Cu$_2$F$_6$K$_2$N$_2$Na$_2$O$_{10}$; Calcd 587.0923) (Figure S9). But for a 1:100 molar ratio peak at a m/z value of 819.4127 could be assigned to the mononuclear species [Cu(L1)(3,5-DTBCH)$_2$(CH$_3$OH)(H$_2$O)-Na]$^+$ (C$_{44}$H$_{65}$CuN$_2$NaO$_7$; Calcd 819.3985) (Figure S10) indicating at the collapse of the dinuclear fragment at high 3,5-DTBCH$_2$ concentrations.

Solution of **3** in MeOH gave a medium intensity peak at m/z = 413.2657 for [Cu$_2$(L1)(OH)(C$_6$H$_5$COO)$_3$(CH$_3$OH)-2Na]$^+$ (C$_{37}$H$_{37}$Cu$_2$N$_2$Na$_2$O$_9$; Calcd 413.5429) (Figure S11). Whereas a mixture of **3** and 3,5-DTBCH$_2$ in 1:100 molar ratio in MeOH resulted peaks at m/z = 243.1381 and 463.2868 for [3,5-DTBQ-Na]$^+$ and [(3,5-DTBQ)$_2$-Na]$^+$, respectively (Figure S12) confirming formation of free quinone unit. Characteristic catalyst-partially oxidized substrate aggregate [Cu$_2$(L1)(OH)(C$_6$H$_5$COO)$_2$(DTSQ)$_2$(H$_2$O)-2H]$^{2+}$ (C$_{37}$H$_{37}$Cu$_2$N$_2$Na$_2$O$_9$; Calcd 544.1918) was found as a low intensity peak at m/z = 544.3038.

MeOH solution of **4** gave peak at m/z = 545.0192 for the diagnostic {Cu$_2$} fragment [Cu$_2$(L1)(OH)(CH$_3$COO)$_2$(H$_2$O)-(2H)Na]$^+$ (C$_{20}$H$_{30}$Cu$_2$N$_2$NaO$_7$; Calcd 545.0386) (Figure S13). When mixed with 3,5-DTBCH$_2$ in MeOH in 1:100 molar ratio the species with coordinated semiquinonate form of the substrate as [Cu$_2$(L1)(OH)(CH$_3$COO)$_2$(DTSQ)$_2$(CH$_3$OH)$_2$-2K]$^{2+}$ (C$_{49}$H$_{72}$Cu$_2$K$_2$N$_2$O$_{12}$; Calcd 543.1461) was obtained as a low intensity peak at m/z = 543.3044 (Figure S14).

Cyclic Voltammetric Traces in Solution

The redox sensitivity of the complexes required for the catalytic oxidation of 3,5-DTBCH$_2$ were examined by cyclic voltammetry measurements. This gave an idea about the

involvement of redox active ~~substrate~~ species during catalysis. The same MeOH medium was chosen for the measurement in a N_2 atmosphere with TBAP supporting electrolyte, platinum working electrode, platinum wire counter electrode and Ag/AgCl reference electrode (Figure S15). Bare HL1 showed a reduction peak at −0.898 V which was shifted upon complex formation in the −0.698 to −0.888 V range *vs.* Ag/AgCl for **1–4** and were most likely for the reduction of the bare and Cu^{II} bound C=N bond. An oxidative response at 0.733 V *vs.* Ag/AgCl appeared for free HL1 and in the 0.708 to 0.860 V range for metal bound ligand in **1–4**. The nature of the voltammograms were in favor of only ligand-centered redox processes without showing any change in oxidation state of the involved metal ion centers from Cu^{II} to Cu^{I} during the oxidation of 3,5-DTBCH$_2$ to 3,5-DTBQ.

EPR Sensitive Species in Solution

X-band EPR spectra of MeOH solutions of **1-4** at 298 K showed very weak isotropic signals at $g \sim 2.0$ and a second one at $g \sim 4.0$ indicating the presence of ligand bound $\{Cu_2\}$ entities in solution (Figure S16 left and Figure 13 left). In particular, the signals at $g \sim 4.0$ were attributable to $\{Cu_2\}$ species (*cf.* the low-field $\Delta M_S = \pm 2$ features) as indicated in HRMS analysis. The isotropic g parameters (g_{iso}) could not be ascertained unambiguously due to the weak and noisy signals around $g \sim 2.0$. The g values associated with the $\Delta M_S = \pm 2$ transitions were found to be 4.25, 4.26, 4.25 and 4.28 respectively for **1-4**. The EPR spectra were recorded after 10 min of mixing of **1-4** and 3,5-DTBCH$_2$ in 1:100 molar ratio in MeOH at 298 K (Figures S16 right and 13 right). The spectra for **1**, **3** and **4** showed sharp signals at g = 2.01, 2.00 and 2.00 respectively confirming the generation of organic free radical in solution.[47] Repeat scans in 3420-3475 G range, keeping the number of data points the same as before, showed splitting of these signals into two with additional lower intensity shoulders to the right in all the three cases. This observation of doubly split signal justifies the presence of an unpaired electron on C4 of DTSQ bearing a single hydrogen atom.[48] The signals appearing as shoulders arise from a C=N centered radical in L1 and L2. An unpaired electron on the imine carbon would have given a six line spectrum. Clear resolution was obscured in the presence of a strong DTSQ radical signal. An interesting observation was made in the EPR spectrum of **2** with 100 equivalents of 3,5-DTBCH$_2$. It was different from that of the complex alone giving $g_{iso} = 2.15$ signal of much higher intensity (Figure 13 right). This was due to the formation of catechol bound mononuclear Cu^{II} species as evidenced from mass analysis.
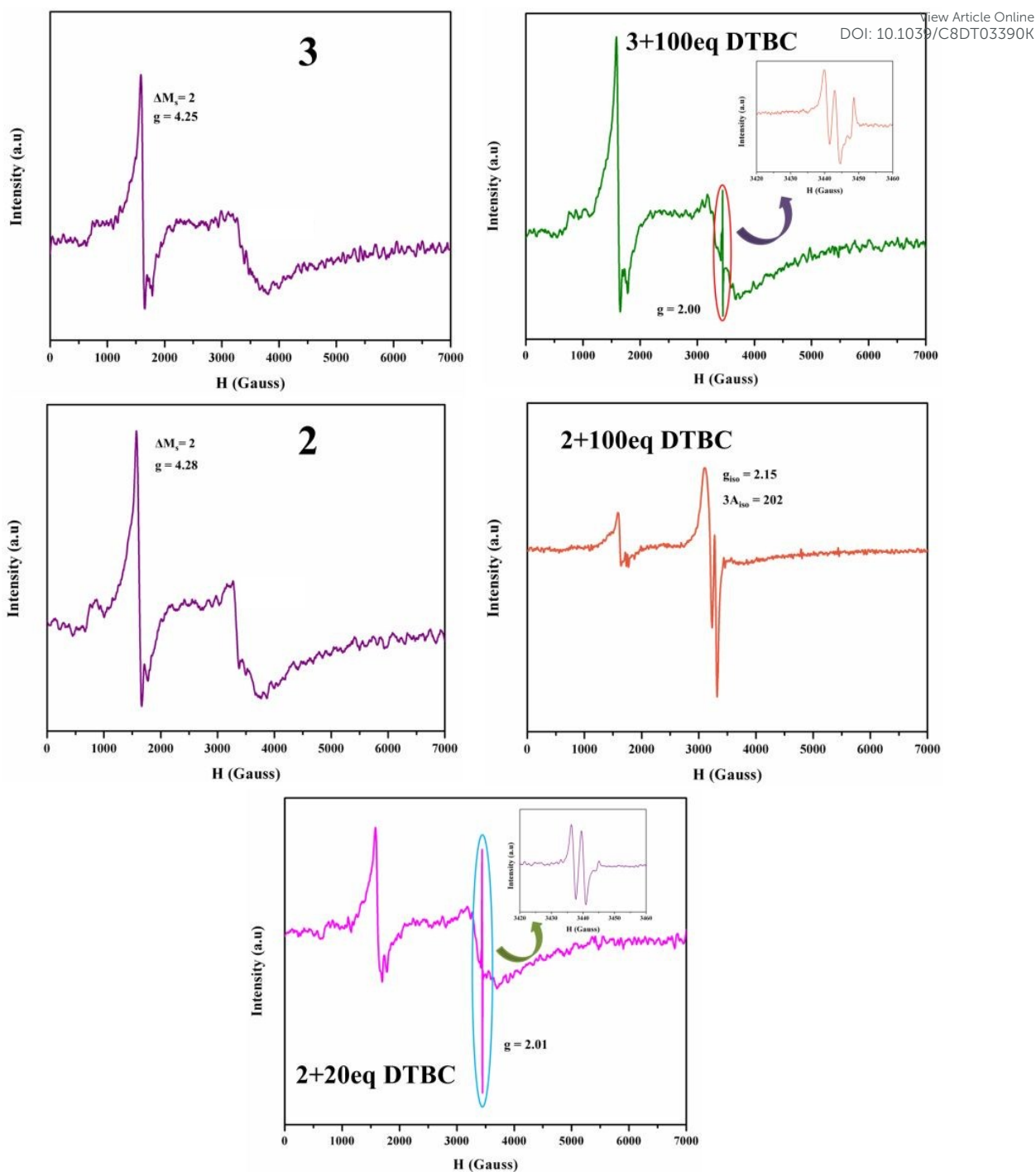
Figure 13 EPR spectra of **3** and **2** (left), mixtures of **3** and **2** with 3,5-DTBCH$_2$ in 1:100 molar ratio (right) and mixture of **2** with 3,5-DTBCH$_2$ in 1:20 molar ratio (bottom) in MeOH at 298 K

As analysis of reaction rate data for **2** gave highest rate for 20 equivalents of the substrate, EPR measurements were performed on a mixture of **2** and 3,5-DTBCH$_2$ in a 1:20 molar ratio in MeOH (Figure 13 bottom). The spectrum showed a strong and sharp signal at $g = 2.01$ indicating the presence of organic radical species and a doubly split signal with lower intensity shoulders similar to **1**, **3** and **4**.

Probable Mechanism for Catechol Oxidation

In order to establish a reasonable course of the metal ion complex mediated oxidation reaction, we need to know whether the O_2 in air reduces to H_2O or H_2O_2 during the process. The estimation of H_2O_2 formed in the medium was performed by a modified iodometric titration procedure accelerated by molybdate ions. The oxidation of I^- to I_2 followed by the generation of I_3^- was apparent from the UV-vis spectral study of the solution obtained after work-up indicating the generation of H_2O_2 as identified by others.[8] A significant amount of H_2O_2 is found to be accumulated in the reaction medium in all the studied cases (Figure S17).
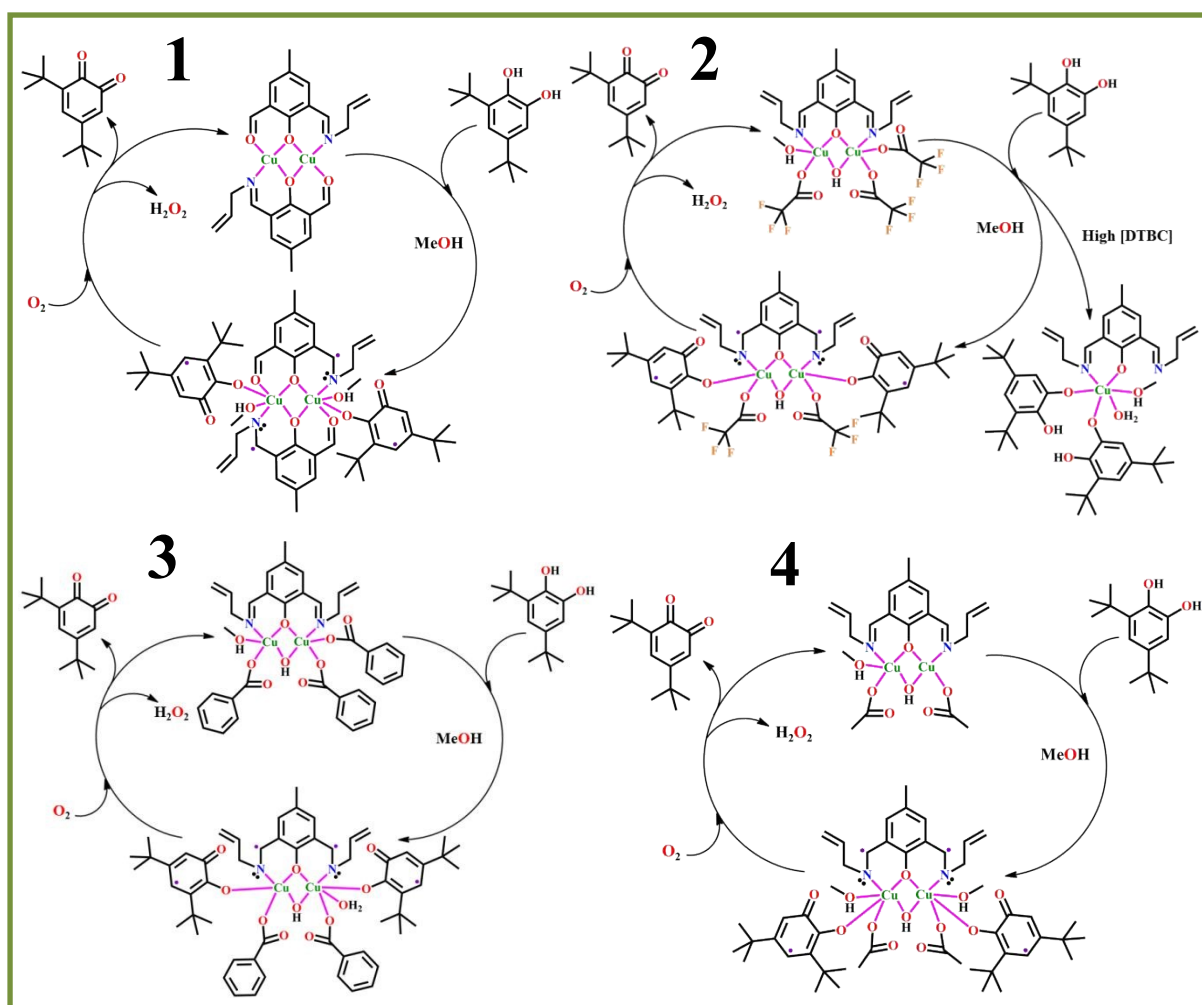
Scheme3 Proposed course of catalytic oxidation of 3,5-DTBCH$_2$

From HRMS, CV and EPR analysis a mechanistic pathway can be tentatively proposed for the catalytic oxidation of 3,5-DTBCH$_2$ to 3,5-DTBQ by **1-4**. In MeOH solution the active species like $\{Cu_2(L2)_2\}$, $\{Cu_2(L1)(OH)(CF_3COO)_3(CH_3OH)\}$, $\{Cu_2(L1)(OH)(C_6H_5COO)_3(CH_3OH)\}$ and $\{Cu_2(L1)(OH)(CH_3COO)_2(H_2O)\}$ were present to bind 3,5-DTBCH$_2$ giving $\{Cu_2(L2)_2(DTSQ)_2(CH_3OH)_2\}$,

Dalton Transactions

$\{Cu_2(L1)(OH)(CF_3COO)_2(DTSQ)_2\}$, $\{Cu_2(L1)(OH)(C_6H_5COO)_2(DTSQ)_2(H_2O)\}$ and $\{Cu_2(L1)(OH)(CH_3COO)_2(DTSQ)_2(CH_3OH)_2\}$ respectively for **1**, **2**, **3** and **4**. In all these cases the generation of semiquinone radical species and metal ion bound imine-centered radical fragments were detected from EPR signals. No reduction peak corresponding to the conversion of Cu^{II} to Cu^I is observed for **1-4** in MeOH solution and each ligand imine bond accepts an electron to remain in reduced state.[47] The lone electron is later accepted by a dioxygen molecule completing the catalytic cycle releasing 3,5-DTBQ and H_2O_2 (Scheme 3). Thus the used pro-radical system is expected to exploit ligand redox activity centered on the imine groups for catalytic activity. Complex **2** in the presence of high concentration of $DTBCH_2$ breaks down to catechol bound mononuclear Cu^{II} species $\{Cu(L1)(3,5\text{-}DTBCH)_2(CH_3OH)(H_2O)\}$ as indicated by HRMS, which was catalytically inactive inhibiting the catalytic oxidation.

Comparison of Catalytic Activity

With respect to the determined catalytic turn over number, k_{cat} the reactivity order of the complexes for the oxidation of 3,5-$DTBCH_2$ follow the trend **4 > 2 > 3 > 1**. From HRMS analysis it was found that in solution the parent ligand bound $\{Cu_2\}$ fragments predominate over other species obtained through crystallization. The highest k_{cat} value in the series for **4** is evident from the fact that it provides four $\{Cu_2\}$ fragments in solution because its unit cell consists of two $[Cu_5]$ units. The presence of double phenoxido-bridges in **1** rendered it least active possibly due to the availability of less room for substrate binding.[49] Monodentate coordination of two different carboxylate groups in **2** and **3** resulted two types of $\{Cu_2\}$ fragments showing difference in catalytic activity. The Michaelis-Menten constant K_M shows the concentration of the catechol when the reaction velocity is equal to one half of the maximal velocity for the reaction and also it is a measure of binding affinity of the catechol molecules to the $\{Cu_2\}$ fragments. When K_M value is less it indicates a greater binding affinity and *vice-versa*. In this work the K_M value for **2** is less than that for **3** indicating superior binding affinity of fragments generated from **2**. The observed difference in the k_{cat} values can be explained by considering the rate determining step as the transfer of electron from the substrate to the imine functions of the ligand through the Cu^{II} centers. Trifluroacetate groups, having electron withdrawing fluorine atoms, were responsible for withdrawal of electron density from Cu^{II} centers compared to benzoate group bound fragments. The coordination of trifluroacetate groups facilitate the transfer of electrons from catechol and semiquinone molecules to bound imine functions *via* Cu^{II} centers in **2**, compared

to **3** with attached to benzoate groups, resulting in higher k_{cat} value. A higher k_{cat} value indicates that more substrate molecules were turned over per second. The catalytic efficiency can also be compared from the k_{cat}/K_M values and a catalyst with high k_{cat} and low K_M values is more efficient in this regard. The effect of the electron-withdrawing nature of the CF_3COO^- group is further exemplified by the fact that **2** has the highest catalytic efficiency (k_{cat}/K_M) in the group. Of the four complexes studied only **2** showed substrate inhibition, most probably due to the failure of trifluoroacetate group to stabilize the $\{Cu_2\}$ species in the presence of a large excess of 3,5-DTBCH₂. Oxidation of 3,5-DTBCH₂ by **1**, **3** and **4** took place in a single phase as confirmed from the first-order exponential growth of 3,5-DTBQ over time.

Paths for Coordination Aggregation

Two important and competitive paths have been identified for the first time in this work: metal ion coordination induced ligand arm hydrolysis and hydroxide ion coordination driven self-aggregation of the initially formed fragments. Varying reaction conditions and the presence of different carboxylate anions leads to the stabilization of two types of $\{Cu_2\}$ fragments A and B (Scheme 4).
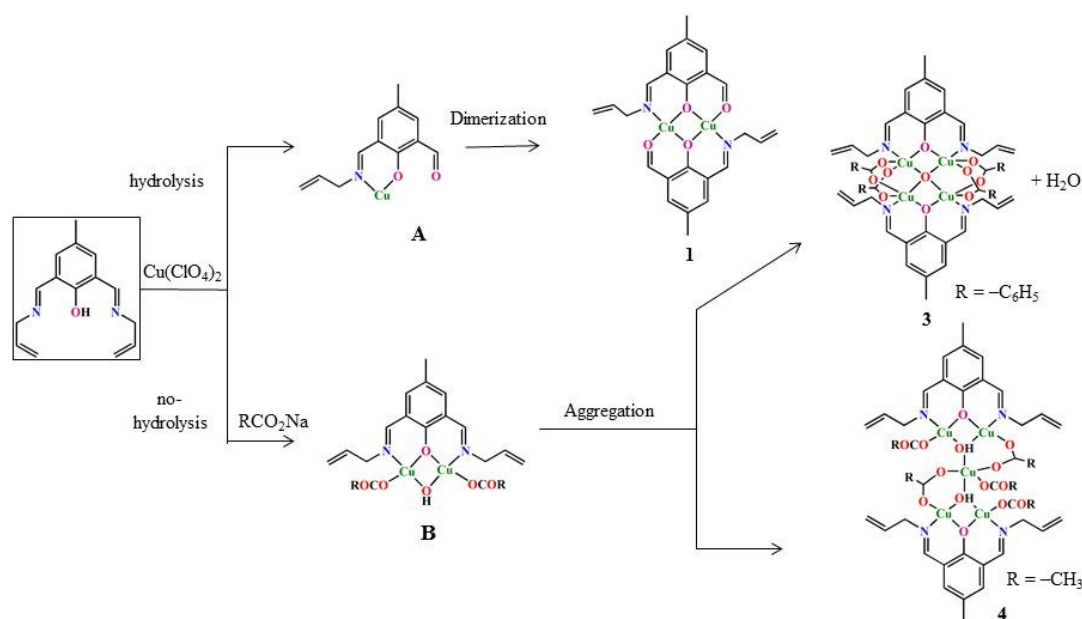
Scheme 4 Proposed routes of aggregation in solution followed by crystallization

In the absence of any carboxylate anion the reaction of HL1 with Cu^{II} ion triggered a single imine arm hydrolysis to produce $\{Cu(L2)\}$ fragment A, whose dimerization in solution resulted **1**. Reaction in the presence of carboxylate ions provided their termination coordination and *in situ* generated HO^- ions were utilized to bridge two Cu^{II} centers in

$[Cu_2(\mu–L1)(\mu–OH)(O_2CR)_2]$ fragment B. Trifluoroacetate, benzoate and acetate anions, showing varying intermetallic clipping ability, were responsible for two different types of homometallic aggregations as $[Cu_4]$ complexes **2** and **3**, and $[Cu_5]$ complex **4**.

Conclusions

While examining the coordination reactivity pattern of HL1 with Cu^{II} in the absence or presence of three ancillary bridges a new family of compounds have been recognized showing characteristic physical and biophysical behaviors. Ancillary ligands were utilized to inhibit the ligand-arm hydrolysis and trap the reactive fragments. Formation of the aggregated products avoiding ligand-arm hydrolysis is reliant on the choice of solvent system and carboxylate bridges for the self-assembly of the preformed $\{Cu_2\}$ units. In these reactions, coordination and bridging of more than one type of smaller groups drive the resulting reaction paths and products. The presence of carboxylate group was crucial to modulate the course of aggregation. In the absence of these carboxylate anions, the available perchlorate ions from metal ion salts were responsible to hydrolyze the imine arm of the ligand to yield **1**. The presence of carboxylate anions on the other hand prevent this path and take part in coordination aggregation. Externally added $CF_3CO_2^-$ and $PhCO_2^-$ ions thus showed preference for the inter-fragment reaction $2\{Cu_2L1(OH)\} \rightarrow \{Cu_4(\mu_4–O)L1_2\} + H_2O$ in **2** and **3**. Use of CH_3COO^- ions on the other hand, lead to the trapping of central Cu^{II} ion by two such $\{Cu_2L1(OH)\}$ fragments to provide **4** in a different sequence of aggregation. This emphasizes the role of CH_3COO^- ions for the self-assembly of two L1 bound $\{Cu_2\}$ fragments, responsible for the trapping of the central Cu^{II} center. The magnetic properties of **2**, **3** and **4** are dominated by strong antiferromagnetic exchange interactions, consistent with the presence of the Cu−O−Cu phenoxido−bridges. From their bio-relevant behavior, all the complexes act as efficient catalyst for the aerobic oxidation of 3,5-DTBCH$_2$ to 3,5-DTBQ in MeOH and their reactivity order is **1** < **3** < **2** < **4**. For complex **2**, inhibition of reaction by substrate molecules was observed at high 3,5-DTBCH$_2$ concentration due to formation of an inactive mononuclear copper complex–catechol adduct as confirmed by HRMS analysis and EPR study. ESI−MS also proved that in solution the $\{Cu_2\}$ fragment is the active catalyst for oxidation of 3,5-DTBCH$_2$ to 3,5-DTBQ. Further work in the same line is currently in progress in our laboratory to grow larger cages supported by the *in situ* generated, metal salt supplied and externally added anions.

Electronic Supplementary information

X-ray crystallographic data in CIF format, Scheme S1–S2, Figures S1−S17, Tables S1. CCDC 1857609, 1857607, 1857608 and 1857610.contain the supplementary crystallographic data in CIF format for complexes **1−4**.

Author Information

Corresponding Author

*E-mail: dray@chem.iitkgp.ac.in. Tel: (+91) 3222-283324. Fax: (+91) 3222-82252.

ORCID

Debashis Ray: 0000-0002-4174-6445

Conflict of interest

The authors declare no competing financial interest

References

1 E. M. Shepard and D. M. Dooley, *Acc. Chem. Res.*, 2015, **48**, 1218–1226.

2 C. M. Chang, V. J. Klema, B. J. Johnson, M. Mure, J. P. Klinman and C. M. Wilmot, *Biochemistry*, 2010, **49**, 2540–2550.

3 I. A. Koval, K. van der Schilden, A. M. Schuitema, P. Gamez, C. Belle, J.-L. Pierre, M. L. Lueken, B. Krebs, O. Roubeau and J. Reedijk, *Inorg. Chem.*, 2005, **44**, 4372–4382.

4 M. R. Halvagar, P. V. Solntsev, H. Lim, B. Hedman, K. O. Hodgson, E. I. Solomon, C. J. Cramer and W. B. Tolman, *J. Am. Chem. Soc.*, 2014, **136**, 7269.

5 H. Sun, K. Harms and J. Sundermeyer, *J. Am. Chem. Soc.*, 2004, **126**, 9550–955.

6 M. Prudencio, A. S. Pereira, P. Tavares, S. Besson, I. Cabrito, K. Brown, B. Samyn, B. Devreese, J. Van Beeumen, F. Rusnak, G. Fauque, J. J. G. Moura, M. Tegoni, C. Cambillau and I. Moura, *Biochemistry*, 2000, **39**, 3899–3907.

7 S. K. Dey and A. Mukherjee, *Coord. Chem. Rev.*, 2016, **310**, 80−115.

8 K. Chattopadhyay, B. K. Shaw, S. K. Saha and D. Ray, *Dalton Trans.*, 2016, **45**, 6928−6938.

9 M. Pait, E. Colacio and D. Ray, *Polyhedron*, 2015, **88**, 90-100.

10 A. Escuer, G. Vlahopoulou, S. P. Perlepes and F. A. Mautner, *Inorg. Chem.*, 2011, **50**, 2468–2478.

11 M. Sarkar, R. Clerac, C. Mathoniere, N. G. R. Hearns, V. Bertolasi and D. Ray, *Inorg. Chem.*, 2010, **49**, 6575–6585.

12 E. Bosch and C. L. Barnes, *J. Coord. Chem.*, 2003, **56**, 329–336.

13 H. Liu, H. Wang, H. Wu and D. Niu, *J. Coord. Chem.*, 2005, **58**, 1345–1349.

14 A. K. Ghosh, M. Pait, R. Clérac, C. Mathonière, V. Bertolasi, A. Bauza, A. Frontera, K. Pramanik and D. Ray, *Dalton Trans.*, 2014, **43**, 4076–4085.

15 H. Kumari, A. V. Mossine, S. R. Kline, C. L. Dennis, D. A. Fowler, S. J. Teat, C. L. Barnes, C. A. Deakyne and J. L. Atwood, *Angew. Chem., Int. Ed.*, 2012, **51**, 1452–1454.

16 R. R. Gagne, C. L. Spiro, T. J. Smith, C. A. Hamann, W. R. Thies and A. D. Shiemke, *J. Am. Chem. Soc.*, 1981, **103**, 4073–4081.

17 *SAINT, SMART and XPREP*, Siemens Analytical X-ray Instruments Inc., Madison, WI, 1995.

18 G. M. Sheldrick, *SHELXS-2014*, University of Göttingen, Göttingen, Germany, 2014.

19 G. M. Sheldrick, Crystal structure refinement with SHELXL. *Acta Crystallogr.,Sect. A: Found. Crystallogr.* 2008, **64**, 112−122.

20 L. J. Farrugia, *WinGX-Version 2014.1*, *J. Appl. Crystallogr.* 2012, **45**, 849−854.

21 G. M. Sheldrick, *SADABS Software for Empirical Absorption Correction*, University of Göttingen, Institute für Anorganische Chemieder Universität, Göttingen, Germany, 1999−2003.

22 Z. Otwinowski and W. Minor, Processing of X-ray Diffraction Data Collected in Oscillation Mode, in *Methods in Enzymology: Macromolecular Crystallography, part A*, ed. Carter Jr, C. W.; Sweet, R. M. Academic Press, New York, 1997, **276**, 307–326.

23 R. H. Blessing, *Acta Crystallogr., Sect. A: Found. Crystallogr.*, 1995, **51**, 33–37.

24 A. Altomare, M. C. Burla, M. Camalli, G. L. Cascarano, C. Giacovazzo, A. Guagliardi, A. G. G. Moliterni, G. Polidori and R. J. Spagna, *J. Appl. Crystallogr.*, 1999, **32**, 115–119.

25 M. Nardelli, *J. Appl. Crystallogr.*, 1995, **28**, 659.

26 L. J. Farrugia, *J. Appl. Crystallogr.*, 1999, **32**, 837–838.

27 *DIAMOND, Visual Crystal Structure Information System, version 3.1*, Crystal Impact: Bonn, Germany, 2004.

28 A. Neves, L. M. Rossi, A. J. Borotoluzzi, B. Szpoganicz, C. Wiezbicki, E. Schwingel, W. Haase and S. Ostrovsky, *Inorg. Chem.*, 2002, **41**, 1788–1794.

29 K. Nakamoto, *Infrared and Raman Spectra of Inorganic and coordination compounds*, Wiley, New York, 4th edition, 1986.

30 A. Ozarowski, I. B. Szymanska, T. Muziol and J. Jezierska, *J. Am. Chem. Soc.*, 2009, **131**, 10279–10292.

31 G. B. Deacon and R. J. Phillips, *Coord. Chem. Rev.*, 1980, **33**, 227–250.

32 G. Tabbì, A. Giuffrida and R. P. Bonomo, *J. Inorg. Biochem.*, 2013, **128**, 137–145.

33 A. Biswas, L. K. Das, M. G. B. Drew, C. Diaz and A. Ghosh, *Inorg. Chem.*, 2012, **51**, 10111–10121.

34 A. W. Addison, T. N. Rao, J. Reedijk, J. V. Rijn and G. C. Verschoor, *J. Chem. Soc. Dalton Trans.*, 1984, 1349–1356.

35 Z. Johan and J. Hak. *Chem. Erde*, 1958, **20,** 49–50.

36 D. Zhang, H. Berger, R. K. Kremer, D. Wulferding, P. Lemmens and M. Johnsson, *Inorg. Chem.*, 2010, **49**, 9683–9688.

37 A. K. Ghosh, R. Clérac, C. Mathoniére and D. Ray, *Polyhedron*, 2013, **54**, 196–200.

38 M. Sarkar, R. Clerac, C. Mathoniere, N. G. R. Hearns, V. Bertolasi and D. Ray, *Inorg.Chem.*,2011, **50**, 3922–3933.

39 N. F. Chilton, R. P. Anderson, L. D. Turner, A. Soncini and K. S. Murray, *J. Comput. Chem.*, 2013, **34**, 1164–1175.

40 X. Wang, K.-Q. Zhao, M. R. J. Elsegood, T. J. Prior, X. Liu, L. Wu, S. Sanz, E. K. Brechin and C. Redshaw, *RSC Adv.*, 2015, **5**, 57414–57424.

41 M. S. Jana, S. Dey, J. L. Priego, R. Jiménez-Aparicio, T. K. Mondal and P. Roy, *Polyhedron*, 2013, **59**, 101–106.

42 L. K. Thompson, S. K. Mandal, S. S. Tandon, J. N. Bridson and M. K. Park, *Inorg. Chem.*, 1996, **35**, 3117–3125.

43 F. Tuna, L. Patron, Y. Journaux, M. Andruh, W. Plass and J.-C. Trombe, *J. Chem. Soc., Dalton Trans.*, 1999, 539–545.

44 M. Das, G. A. Craig, D. Escudero, M. Murrie, A. Frontera and D. Ray, *New J. Chem.*, 2018, DOI 10.1039/C8NJ02131G

45 A. Rompel, H. Fischer, D. Meiwes, K. Buldt-Karentzopoulos, A. Magrini, C. Eicken, C. Gerdemann and B. Krebs, *FEBS Lett.*, 1999, **445**, 103–110.

46 E. Monzani, G. Battaini, A. Perotti, L. Casella, M. Gullotti, L. Santagostini, G. Nardin, L. Randaccio, S. Geremia, P. Zanello and G. Opromolla, *Inorg. Chem.*, 1999, **38**, 5359–5369.

47 T. Ghosh, J. Adhikary, P. Chakraborty, P. K. Sukul, M. S. Jana, T. K. Mondal, E. Zangrando and D. Das, *Dalton Trans.*, 2014, **43**, 841–852.

48 S. M. Yi, K. V. Narasimhulu, R. I. Samoilova, R. B. Gennis and S. A. Dikanov, *J. Biol. Chem.*, 2010, **285**, 18241–18251.

49 J. Mukherjee and R. Mukherjee, *Inorg. Chim. Acta*, 2002, **337**, 429–438.

Table of Contents

Strategic Synthesis of [Cu$_2$], [Cu$_4$] and [Cu$_5$] Complexes: Inhibition and Triggering of Ligand Arm Hydrolysis and Self-aggregation by Chosen Ancillary Bridges

Manisha Das,[a] Angelos B. Canaj,[b] Valerio Bertolasi,[c] Mark Murrie,[b] Debashis Ray[*a]

A new family of Cu^{II}-based coordination aggregates is synthesized from HL1 with Cu(ClO$_4$)$_2$·6H$_2$O in absence and presence of a group of carboxylates.